DISSERTATION

L-Type Calcium Channel Structure and Function: Mechanisms of Gating and Signaling in Skeletal Muscle

Submitted by

Christina M. Wilkens

Department of Anatomy and Neurobiology

In Partial Fulfillment of the Requirements

for the Degree of Doctor of Philosophy

Colorado State University

Fort Collins, Colorado

Spring, 2002

COLORADO STATE UNIVERSITY

November 6, 2001

WE HEREBY RECOMMEND THAT THE DISSERTATION PREPARED UNDER OUR SUPERVISION BY CHRISTINA M. WILKENS ENTITLED "L-TYPE Ca^{2+} CHANNEL STRUCTURE AND FUNCTION: MECHANISMS OF GATING AND SIGNALING IN SKELETAL MUSCLE" BE ACCEPTED AS FULFILLING, IN PART, REQUIREMENTS FOR THE DEGREE OF DOCTOR OF PHILOSOPHY

Committee on Graduate Work

Sue C. Kinnamon 11-26-01

12-5-01

Kathy M Patti 12/6/01

11/27/01

Adviser

12/6/01

Department Head

ABSTRACT OF DISSERTATION

L-TYPE Ca^{2+} CHANNEL STRUCTURE AND FUNCTION: MECHANISMS OF GATING AND SIGNALING IN SKELETAL MUSCLE

L-type channels in muscle function both as voltage-gated Ca^{2+} channels and as voltage sensors for excitation-contraction (EC) coupling. Potentiation of Ca^{2+} channels results in a net increase in Ca^{2+} influx, providing a potent means for regulation of Ca^{2+} dependent cellular processes. A defining property of L-type channels is their potentiation by both dihydropyridine agonists and strong depolarization. In contrast, non L-type channels are potentiated by neither agonist nor depolarization, suggesting that these two processes may be linked. Here we have tested whether the mechanisms of agonist- and depolarization-induced potentiation in the cardiac L-type channel (α_{1C}) are linked. We found that the mutant L-type channel GFP-α_{1C}(TQ→YM), bearing the mutations T1066Y and Q1010M, was able to undergo depolarization-induced potentiation but not potentiation by agonist. Conversely, the chimeric channel GFP-CACC was potentiated by agonist but not strong depolarization. These data indicate that the mechanisms of agonist- and depolarization-induced potentiation of α_{1C} are distinct. Since neither GFP-CACC nor GFP-CCAA was potentiated significantly by depolarization, no single repeat

of the α_{1C} can be responsible for depolarization-induced potentiation. Interestingly, GFP-CACC displayed a low channel open probability similar to that of α_{1C}, but could not support depolarization-induced potentiation, demonstrating that a relatively low open probability alone is not sufficient for depolarization-induced potentiation to occur. Thus, depolarization-induced potentiation may be a global channel property requiring participation from all four homologous repeats.

The L-type channel in skeletal muscle (α_{1S}) functions primarily as a voltage sensor for EC coupling. The α_{1S} undergoes a conformational change in response to membrane depolarization, which causes the ryanodine receptor (RyR) in the sarcoplasmic reticulum to release intracellular Ca^{2+} stores, independent of Ca^{2+} entry through the channel. The II-III loop of α_{1S} is responsible for bi-directional signaling interactions with the skeletal RyR (RyR1): transmitting the orthograde, EC coupling signal to RyR1 and receiving a retrograde, Ca^{2+} current-enhancing signal from RyR1. Previous reports had argued for the importance of two distinct regions of the skeletal II-III loop (residues R681-L690 and residues L720-Q765, respectively), claiming for each a key function in DHPR-RyR1 communication. To address whether residues 720-765 of the α_{1S} II-III loop are sufficient to enable bi-directional signaling with RyR1, we constructed a chimera (SkLM) having rabbit skeletal (Sk) α_{1S} sequence except for a II-III loop (L) from the α_1 subunit of the house fly, *Musca domestica* (M). The *Musca* II-III loop (75% dissimilarity to α_{1S}) has no similarity to α_{1S} in the regions R681-L690 and L720-Q765. Whole-cell patch clamp analysis of SkLM expressed in dysgenic myotubes (which lack endogenous α_{1S} subunits) showed that this construct was unable to mediate bi-directional signaling despite normal surface expression levels and correct junctional targeting (colocalization

with RyR1). Introducing rabbit α_{1S} residues L720-L764 into the *Musca* II-III loop of SkLM completely restored bi-directional signaling, indicating that this 45 residue "critical domain" is likely to be the only sequence of the α_{1S} II-III loop required for bi-directional coupling.

Christina M. Wilkens
Department of Anatomy and Neurobiology
Colorado State University
Fort Collins, Colorado 80523
Spring, 2002

TABLE OF CONTENTS

OVERVIEW

Voltage-gated Ca^{2+} channels are functionally diverse proteins which mediate a variety of cellular processes in both neurons and muscle. These channels exist as multimeric complexes consisting of the main, pore-forming α_1 subunit, as well as the auxilliary β, $\alpha_2\delta$, and, in skeletal muscle, γ subunits. Ca^{2+} channels are traditionally categorized by their α_1 subunits (for which there are ten known genes) into one of five major calcium channel classes (L-, N-, P/Q-, R- and T-type). The L-type channel class consists of the α_{1S} and α_{1C} gene products expressed primarily in skeletal and cardiac muscle, respectively, as well as α_{1D}, which is the predominant L-type Ca^{2+} channel isoform found in neurons.

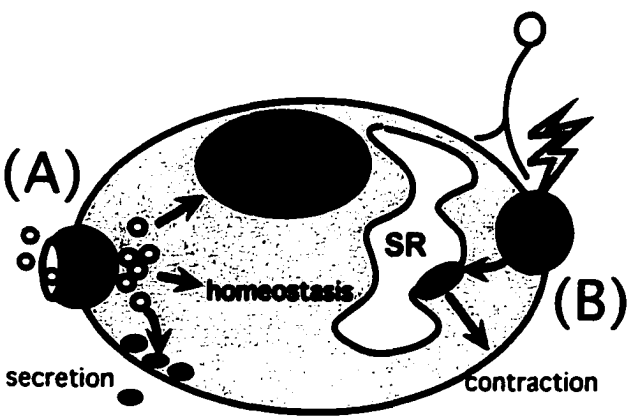

Figure 1. L-type Ca^{2+} channels function both as ion channels and as voltage sensors for muscle contraction. As ion channel pores (A), L-type Ca^{2+} channels (blue) regulate intracellular Ca^{2+} concentrations, and thus influence Ca^{2+}-dependent processes such as gene transcription, homeostasis, and secretion. L-type channels in skeletal muscle function as voltage sensors (B) which transduce electrical excitation of the plasma membrane into fiber contraction via signaling interactions with the sarcoplasmic reticulum (SR) calcium release channel.

L-type channels have two major roles in physiology (Fig. 1). First, these proteins are voltage-gated Ca^{2+} channels which determine intracellular Ca^{2+} concentrations. Ca^{2+} influx through α_{1C} is important in cardiac muscle for determining action potential duration and refractory period, and in neurons, for gene transcription. Second, the L-type channel in skeletal muscle, α_{1S}, functions as a voltage sensor for excitation-contraction (EC) coupling, which transduces electrical excitation of the plasma membrane into eventual fiber contraction. This dissertation considers both roles of L-type channels by examining gating of α_{1C}, and interactions between α_{1S} and other proteins during EC coupling.

Modification of Ca^{2+} influx via changes in the gating of α_{1C} is an important source of regulation in cardiac muscle. One source of modification is potentiation, which stabilizes the open state via an increase in open probability and mean open time, such that Ca^{2+} influx is larger. The α_{1C} normally has a very low open probability and can be potentiated by both strong depolarization and dihydropyridine agonist; in contrast, the non L-type channel α_{1A}, which has a relatively high open probability, is potentiated by neither strong depolarization nor agonist. These observations prompted two questions: first, does potentiation of α_{1C} by agonist and strong depolarization occur via the same molecular pathway? Second, is depolarization-induced potentiation a property of only channels like α_{1C} which have an intrinsically low open probability? In Chapter 1 we have attempted to answer these questions, and to identify the structural determinants underlying depolarization-induced potentiation of α_{1C}.

In skeletal muscle, the L-type channel α_{1S} (also known as the skeletal dihydropyridine receptor, or DHPR) functions as one of two key proteins which mediate

skeletal EC coupling (Fig. 2). The skeletal DHPR is thought to undergo a conformational change in response to membrane depolarization, causing the skeletal ryanodine receptor (RyR1) located in the sarcoplasmic reticulum (SR) to release intracellular Ca^{2+}, which then allows cross-bridge cycling of the actin and myosin filaments to occur. The role of Ca^{2+} entry in RyR1 activation, however, appears to be relatively minor, since skeletal EC coupling occurs in the absence of Ca^{2+} influx through the α_{1S} pore. Instead, EC coupling in skeletal muscle is believed to arise from the direct interaction of the DHPR and RyR1.

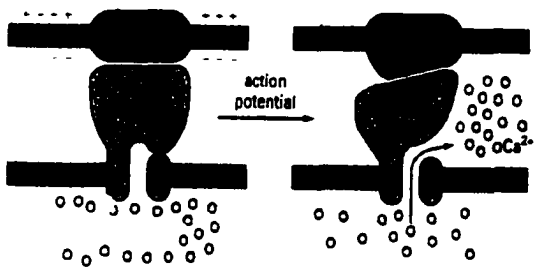

Figure 2. Skeletal excitation-contraction coupling. Electrical excitation of the plasma membrane induces a conformational change in α_{1S}, causing the ryanodine receptor (RyR) located in the sarcoplasmic reticulum to release intracellular Ca^{2+} stores; this Ca^{2+} goes on to trigger cross-bridge cycling of the contractile filaments. [Modified from Alberts et al., 1994.]

Signaling between the DHPR and RyR1 is now known to be bi-directional. In addition to the orthograde, EC coupling signal transmitted from the DHPR to RyR1 (which results in intracellular Ca^{2+} release), RyR1 also transmits a retrograde signal to the DHPR which increases Ca^{2+} current density through the channel. Although we know relatively little about the precise mechanism(s) of orthograde or retrograde signaling, a 46 amino acid region (the "critical domain") of the large intracellular linker connecting homology repeats II and III (skeletal II-III loop) appears to play a major role in signal transduction. However, the role of other regions of α_{1S} in bi-directional signaling, in particular regions of the II-III loop flanking the "critical domain", remain uncertain. Chapter 2 addresses this question by examining the ability of chimeric DHPRs,

containing very divergent II-III loop sequence (α_{1M}) with or without the skeletal "critical domain", to mediate bi-directional signaling with RyR1.

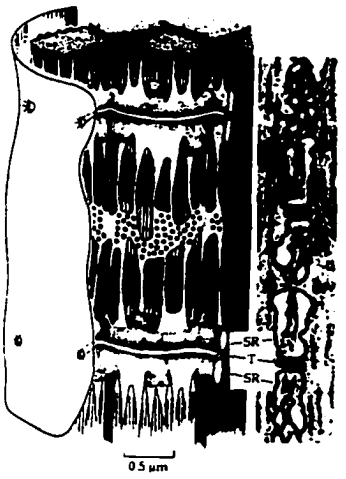

Figure 3. Structure of the skeletal muscle triad junction. The mature skeletal triad junction (left panel) is composed of two terminal sarcoplasmic reticulum cisternae (SR) in colse association with one T-tubule invagination of the plasma membrane (T). The electron micrograph (right panel) illustrates in cross section the precise spatial arrangement of the two membrane systems, which is required for the DHPR and RyR1 proteins to interact. [From Hille, 1992.]

The functional interaction of the skeletal DHPR and RyR1 occurs at specialized regions of the muscle cell known as junctions, which are present in both skeletal and cardiac muscle. In mature skeletal muscle, triad junctions are formed between invaginations of the plasma membrane called transverse tubules and two terminal SR cisternae (Fig. 3), whereas embryonic skeletal muscle consists only of dyad junctions between the outer plasma membrane and the SR. Junctions in cardiac muscle resemble the dyad junctions of embryonic skeletal muscle, and may consist of peripheral couplings between the plasma membrane and the SR, or dyad junctions between a T-tubule and single SR cisterna. Both the α_{1C} and the α_{1S} must be targeted specifically to junctions in order for EC coupling to occur, yet the mechanism for junctional targeting is unknown. Chapter 3 outlines preliminary experiments which have been undertaken in order to identify regions of α_{1S} which are responsible for biosynthesis and targeting of α_{1S}.

Chapter 1 is the result of approximately four years of research performed at Colorado State University, and the text and figures were reproduced from **The Journal of General Physiology, Wilkens et al., 2001, 118, 495-507** by copyright permission of The Rockefeller University Press. Chapter 2 contains text and figures reproduced by copyright permission of The National Academy of Sciences from an original article (**Proceedings of the National Academy of Sciences, Wilkens et al., 2001, 98, 5892-97**), which was a collaboration with Dr. Manfred Grabner at the University of Innsbruck, Austria. Chapter 3 contains some introductory material which was modified with the permission of The American Society for Biochemistry and Molecular Biology from **Journal of Biological Chemistry, Proenza et al., 2000, 275, 23169-74**, but contains otherwise unpublished preliminary data collected by C.M.W.

CHAPTER 1

POTENTIATION OF THE CARDIAC L-TYPE Ca^{2+} CHANNEL (α_{1C}) BY DIHYDROPYRIDINE AGONIST AND STRONG DEPOLARIZATION OCCUR VIA DISTINCT MECHANISMS

Introduction

L-type Ca^{2+} channels show a shift in gating mode in response to either strong depolarization or 1,4-dihydropyridine (DHP) agonist. After a strong depolarization, the channel enters a state of higher open probability (P_o) and long open times which can be detected by a number of different pulse paradigms. For example, after a strong, conditioning depolarization (e.g. +120 mV) followed by a 50-150 ms return to the holding potential, a subsequent, moderate depolarization elicits a Ca^{2+} channel current that is ~2-fold larger than that measured without the conditioning depolarization (Bourinet et al., 1994; Cens et al., 1996, 1998). This effect, which implies an alteration of gating that persists after channel closing, will be designated "depolarization-induced facilitation." Both L- and non L-type channels are also able to undergo another form of prepulse facilitation ("Ca^{2+}/calmodulin-dependent facilitation;" DeMaria et al., 2001; Lee et al., 2000; Zühlke et al., 2000), which differs from depolarization-induced facilitation in that it has a bell-shaped dependence on prepulse potential which arises from a primary

dependence upon Ca^{2+} entry. Ca^{2+}/calmodulin-dependent facilitation appears to depend specifically (Lee et al., 2000) upon the β_{2a} subunit, and does not occur in cells expressing β_1, the isoform present in the dysgenic myotubes used in our study. Unlike Ca^{2+}/calmodulin-dependent facilitation, depolarization-induced facilitation may be related to another form of altered gating observed when a strong depolarization is followed immediately by repolarization to an intermediate potential (Hoshi & Smith, 1987; Pietrobon & Hess, 1990; Kleppisch et al., 1994). This phenomenon, referred to here as depolarization-induced potentiation, results in a mode of gating characterized at the single channel level by high P_o and long channel open times (Fig. 1.1A), which is also

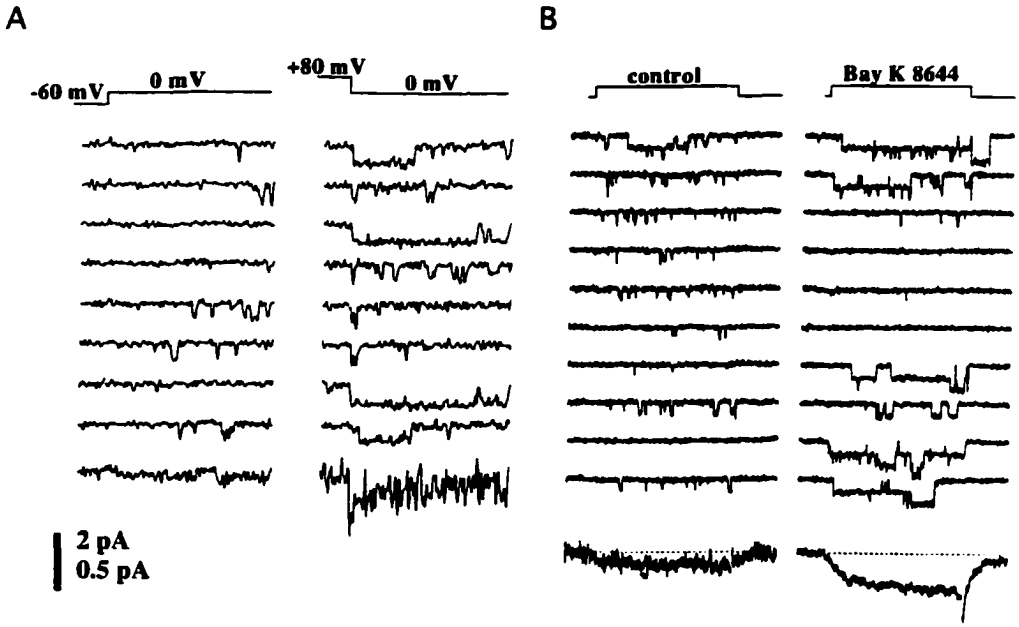

Figure 1.1. Depolarization- and dihydropyridine agonist-induced potentiation of native L-type channels. (A) Unitary currents recorded in 96 mM Ba^{2+} from adrenal chromaffin cells, stepping to 0 mV directly from a holding potential of –60 mV (*left*), or immediately after a 500 ms step to +80 mV *(right)*. (B) A three channel patch recorded in 110 mM Ba^{2+} at ~0 mV from dorsal root ganglion neurons in the absence (*left*) or presence (*right*) of 5 μM Bay K 8644. Ensemble currents (A and B, bottom rows) reflect the increase in open time and P_o caused by agonist and depolarization by the presence of prominent, slowly deactivating tail currents. Individual sweeps are 36 ms for (A) and 130 ms for (B). Vertical bar represents ~2 pA for single channel recordings and ~0.5 pA for ensembles. [Modified from Hoshi & Smith, 1987 (A) and Nowycky et al., 1985 (B).]

referred to as "mode 2" gating (Pietrobon & Hess, 1990). Depolarization-induced potentiation is observed for strong positive prepulses ranging from 50 ms to 1 second in duration, and can last up to 500 ms, depending upon the repolarization potential. As an indication of depolarization-induced entry into mode 2, we have measured whole-cell tail currents upon repolarization to -50 mV immediately after a strong, conditioning depolarization. With this protocol, high P_o and long open times are reflected by an increased tail-current amplitude and slower rate of tail-current decay, respectively. As shown in Figure 1.1B, mode 2 gating of L-type channels is also promoted by DHP agonists (Hess et al., 1984; Nowycky et al., 1985; Hoshi & Smith, 1987). Given the similarities between agonist- and depolarization-induced potentiation, it is important to know the degree to which the two processes are related.

The cardiac L-type channel, α_{1C}, normally exhibits a low P_o of less than 0.05 (Cachelin et al., 1983; Lew et al., 1991) and can be potentiated by both strong depolarization and DHP agonists. By contrast, the neuronal non L-type channel, α_{1A}, exhibits a high P_o of approximately 0.6 (Llinas et al., 1989) and lacks both depolarization-induced facilitation (Bourinet et al., 1994) and DHP-induced potentiation (Sather et al., 1993). These observations suggest the possibility that depolarization- and agonist-induced potentiation can only occur in channels like α_{1C} which have an intrinsically low P_o.

In an attempt to determine whether potentiation of α_{1C} by DHP agonist and strong depolarization occurs via a common pathway we have characterized wild-type and mutant α_{1C} channels and chimeric channels composed of α_{1C} and α_{1A} sequence. The channels were fused at their amino termini to green fluorescent protein (GFP), expressed

in dysgenic myotubes and examined using whole-cell patch clamp. For an α_{1C} in which the agonist binding site was mutated (GFP-α_{1C}(TQ→YM)), 10 μM Bay K 8644 had no significant effect on whole-cell currents, while depolarization-induced potentiation remained intact. A chimeric channel containing repeat II and the I-II linker of α_{1A} sequence embedded in L-type background (GFP-CACC) could not support depolarization-induced potentiation but was potentiated by DHP agonist. Channels containing three (CACC), two (CCAA), or no (α_{1A}) repeats of L-type sequence were not potentiated significantly by depolarization, suggesting that depolarization-induced potentiation cannot be localized to any single channel repeat. Interestingly, despite having a relatively low estimated P_o comparable to that of α_{1C}, GFP-CACC was not potentiated by depolarization, indicating that depolarization-induced potentiation must not be dependent solely on a low P_o. Our results demonstrate that the mechanisms of DHP agonist- and depolarization-induced potentiation of α_{1C} are distinct and that depolarization-induced potentiation may be a global channel property requiring the participation of all four homology repeats.

Materials and Methods

Construction of Chimeric and Mutant α_1 cDNAs: PCR = polymerase chain reaction, nt = nucleotide(s), bp = base pair(s), and A and C denote sequence derived from α_{1A} (Mori et al., 1991) or α_{1C} (Mikami et al., 1989), respectively. An asterisk indicates a restriction site introduced by PCR. The wild-type clones GFP-α_{1C} and GFP-α_{1A} were produced by fusing the α_1 subunit of either the cardiac L-type channel (α_{1C}) or neuronal P/Q-type channel (α_{1A}) at the amino terminus to Green Fluorescent Protein (GFP) as previously

described (Grabner et al., 1998). The GFP tag has been shown not to alter any of the functional properties of the α_{1C} and α_{1A} subunits (Grabner et al., 1998). The clone GFP-α_{1C}(TQ→YM) was created using overlapping PCR mutagenesis (Horton et al., 1989) to replace two residues in the IIIS5 transmembrane domain of α_{1C} (Threonine 1066 and Glutamine 1070), which were previously identified as essential components of the 1,4-dihydropyridine binding site (Mitterdorfer et al., 1996; He et al., 1997), with the corresponding residues of α_{1A} (Tyrosine 1393 and Methionine 1397). Briefly, the SalI* / FspI fragment of α_{1C} was subcloned into pSP72 (Promega), a mutated AflII / AspI fragment of α_{1C} was ligated into the subclone, and the final SalI* / EcoRV fragment carrying the point mutations was ligated into GFP-α_{1C}, thus yielding the clone GFP-α_{1C}(TQ→YM). The α_{1C} / α_{1A} chimera GFP-CACC consisted of repeat II and the I-II linker of α_{1A} contained in α_{1C} background (amino acids 1-426C / 352-671A / 740-2171C). To produce GFP-CACC, the SalI* / EcoRV fragment of α_{1C} was ligated into pSP72. PCR mutagenesis was used to amplify the BamHI* / EcoRI* fragment of α_{1A} sequence (repeat II), which was then ligated into the pSP72/cardiac subclone. Finally, the SalI* / EcoRV chimeric fragment from this subclone was ligated into GFP-α_{1C}. The chimera GFP-CCAA was composed of repeats I and II (including the II-III linker) of α_{1C} and repeats III and IV of α_{1A} (amino acids 1-920C / 1244-2424A). To create GFP-CCAA, the HindIII* / PvuII fragment of chimera AL2 (Grabner et al., 1996) was coligated with the PvuII / BglII fragment of α_{1A} (nt 4216A-5891A) into pSP72. Subsequently, the XhoI / HindIII* fragment of clone AL5 (Grabner et al., 1996) was ligated into this subclone, and the entire XhoI / BglII insert of the resultant subclone was ligated into GFP-α_{1A}, yielding the clone GFP-ALC. The SalI* / AvrII fragment of GFP-

α_{1C} was coligated with the AvrII / AocI fragment of AL5 into the SalI / AocI restriction sites of GFP-ALC, yielding the subclone GFP-C/3A. Finally, the ClaI / AflII fragment of α_{1C} was ligated into GFP-C/3A to yield the final chimera GFP-CCAA. The integrity of all channel constructs was confirmed using automated sequence analysis (Macromolecular Resources, Fort Collins, CO).

Expression and Electrophysiological Analysis of Channels in Dysgenic Myotubes: One week after plating, primary cultures of mouse dysgenic myotubes (Adams et al., 1989), which lack an endogenous α_{1S} subunit (Knudson et al., 1989), were microinjected in single nuclei with cDNAs (200-600 ng/μl) encoding GFP-tagged α_1 subunits. 36-52 hours after injection, expressing myotubes were identified by green fluorescence and used for electrophysiology. Macroscopic Ca^{2+} currents were measured using the whole-cell patch clamp method (Hamill et al., 1981). Whole-cell patch pipettes of borosilicate glass had resistances of 1.5-2.0 MΩ when filled with an internal solution containing 140 mM Cs-aspartate, 10 mM Cs_2EGTA, 5 mM $MgCl_2$, and 10 mM HEPES (pH 7.4 with CsOH). The external bath solution contained 10 mM $CaCl_2$, 145 mM TEA-Cl, and 10 mM HEPES (pH 7.4 with TEA-OH), plus 3 μM tetrodotoxin. Test currents were obtained by stepping from a holding potential of -80 mV to -30 mV for 1 sec (to inactivate endogenous T-type Ca^{2+} current; Adams et al., 1990), to -50 mV for 30-50 ms, to the test potential for 200 ms, to -50 mV for 125 ms, and back to -80 mV. Test currents were corrected for linear components of leak and capacitative currents by digitally scaling and subtracting the average of ten preceding control currents elicited by hyperpolarizing steps (20-40 mV in amplitude) applied from the holding potential. Data were included only for cells in which the maximum voltage error (calculated by the

product of peak inward current and compensated series resistance) was < 10 mV. Except for tail currents, data were sampled at 1 kHz. Tail currents, elicited by repolarizing to -50 mV for 125 ms, were recorded with fast sampling (10 kHz). Tail-current amplitude (I_{tail}) was measured 0.5 ms after the onset of the repolarization from the test pulse to -50 mV. The rate of tail-current decay (τ_{deact}) was measured by fitting tail currents with a single exponential function. Maximal Ca^{2+} conductance (G_{max}) and half-maximal activation potential ($V_{1/2}$) were calculated by fitting peak inward current values with the equation:

$$I = G_{max} * (V-V_{rev}) / \{1 + \exp [-(V-V_{1/2}) / k_G]\} \quad (1)$$

where I is the peak inward Ca^{2+} current measured at the test potential (V), V_{rev} is the reversal potential, and k_G is a slope factor. The values of G_{max} and V_{rev} were then used to calculate normalized conductance as a function of voltage (Figures 1A and 4C) according to the equation: $G(V) = I / \{G_{max} * (V-V_{rev})\}$.

Maximum immobilization-resistant charge movement (Q_{max}) was measured, after addition of 0.5 mM Cd^{2+} and 0.1 mM La^{3+} to the bath, by integration of Q_{on} for a 15 ms test pulse (exponentially rounded with a time constant of 100 μs) to +40 mV. Maximum channel open probability (P_o) was calculated from the average, measured values of $\overline{G_{max}}$ and $\overline{Q_{max}}$ according to the equation:

$$P_o = (q * \overline{G_{max}} * F) / (\gamma * \overline{Q_{max}}' * A) \quad (2)$$

where $\overline{Q_{max}}' = \overline{Q_{max}}$ - average dysgenic charge (2.5 nC/μF; Adams et al., 1990), γ is the single channel conductance in 10 mM Ca^{2+}, assumed to be 4 pS for α_{1A} (Adams et al., 1994), 5.8 pS for α_{1C} (Gollasch et al., 1992), or an average of the two (4.9 pS) for chimeras CACC and CCAA, q is the assumed single channel gating charge (9 e^-; Noceti

et al., 1996), F is Faraday's constant (96,487 C/mol) and A is Avogadro's number (6.023 x 10^{23} e^-/mol).

Several different measures were used to quantify potentiation. For the 1,4-dihydropyridine agonist (+/-)Bay K 8644, one measure was the ratio $I_{max}^{BayK}/I_{max}^{control}$, where the numerator and denominator represent the peak currents elicited by depolarizing test pulses in the presence or absence of drug, respectively. $I_{max}^{control}$ was usually elicited by a V_{test} of approximately +20-30 mV, and I_{max}^{BayK} for a V_{test} 20-30 mV more hyperpolarized. Agonist-induced potentiation was also measured by means of the ratios $I_{tail}^{BayK}/I_{tail}^{control}$ and $\tau_{deact}^{BayK}/\tau_{deact}^{control}$, where the tail current was produced by repolarizing to -50 mV from a V_{test} of +40 mV. Depolarization-induced potentiation was quantified by the ratios $I_{tail}^{+90}/I_{tail}^{+40}$ and $\tau_{deact}^{+90}/\tau_{deact}^{+40}$, where the numerator and denominator were determined from tail currents produced by repolarization to -50 mV after a V_{test} of +90-110 mV or +40 mV, respectively.

Statistical Analysis: Statistical significance was assessed using one-way analysis of variance (ANOVA) and SAS software (Version 8). All data are presented as mean ± S.E.M.

Results

α_{1C} is potentiated by DHP agonist and strong depolarization while α_{1A} is not

Figure 1.2A illustrates representative whole-cell Ca^{2+} currents elicited by depolarizing dysgenic myotubes expressing either GFP-α_{1C} or GFP-α_{1A} to the indicated potentials, followed by repolarization to -50 mV. Based upon steady-state activation calculated from peak currents during the test depolarizations (Fig. 1.2B), both channels

were fully activated by test pulses to +40 mV and above. Consistent with this, the tail currents for GFP-α_{1A} had a similar amplitude and time course following the depolarizations to either +40 or +60 mV (Fig. 1.2A). For GFP-α_{1C}, however, the tail current following the +60 mV depolarization was larger and decayed more slowly than the tail following the +40 mV step. This behavior is an indication that strong depolarization caused α_{1C} channels to enter a mode of gating having longer open times and increased P_o.

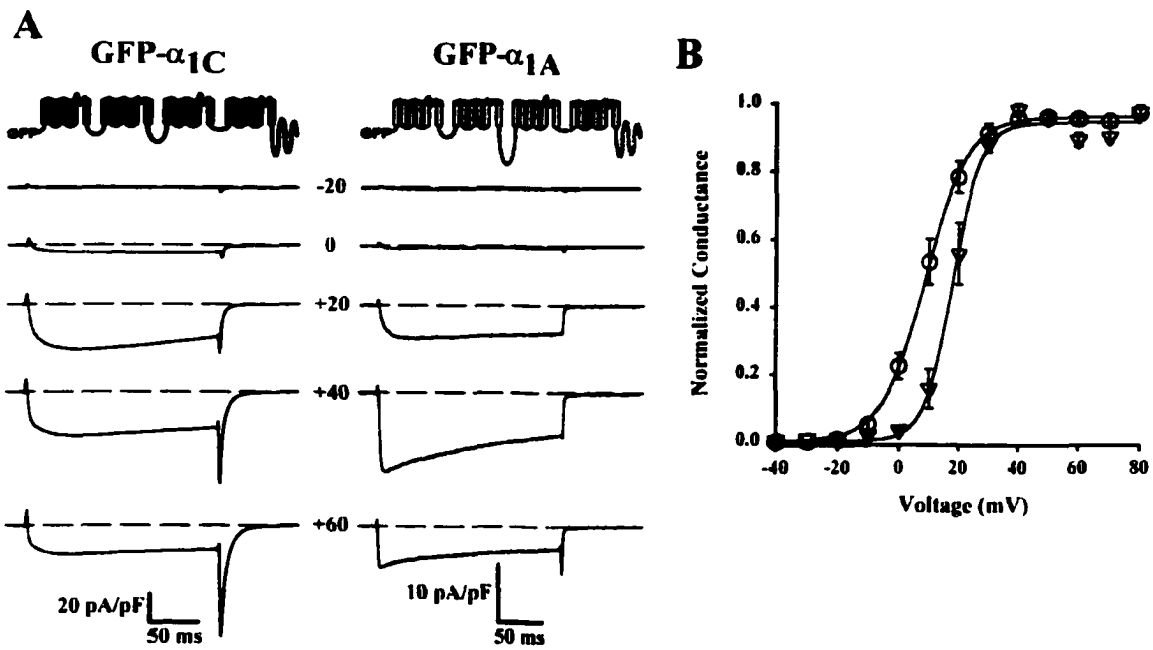

Figure 1.2. Activation of currents produced by GFP-α_{1C} or GFP-α_{1A} expressed in dysgenic myotubes. (A) Representative Ca^{2+} currents elicited by 200 ms depolarizing steps to the indicated test potentials from a holding potential of -80 mV, followed by repolarization to -50 mV. Putative membrane topology for each GFP-tagged channel is indicated, where dark gray and light gray represent α_{1C} and α_{1A} sequence, respectively. (B) Average (+/- SEM) conductance vs. voltage relationships for GFP-α_{1C} (circles; n = 9) and GFP-α_{1A} (inverted triangles; n = 10). The smooth curves represent best fits of the expression $1/\{1 + \exp[-(V-V_{1/2})/k_G]\}$ which yielded the values: GFP-α_{1C}, $V_{1/2}$ = 8 mV, k_G = 7.3 mV; GFP-α_{1A}, $V_{1/2}$ = 19 mV, k_G = 5.1 mV. [From Wilkens et al., 2001a.]

Figure 1.3 compares currents produced by GFP-α_{1C} and GFP-α_{1A} before and after exposure to 10 μM Bay K 8644. For GFP-α_{1A}, application of Bay K 8644 had little effect on either the current elicited by a test depolarization to +20 mV or on the tail current after repolarization (Fig. 1.3A). Likewise, the average, peak current vs. voltage relationship for GFP-α_{1A} was not significantly ($p > 0.1$) affected by the agonist (Fig. 1.3B). By contrast, Bay K 8644 caused a hyperpolarizing shift in the test potential evo-

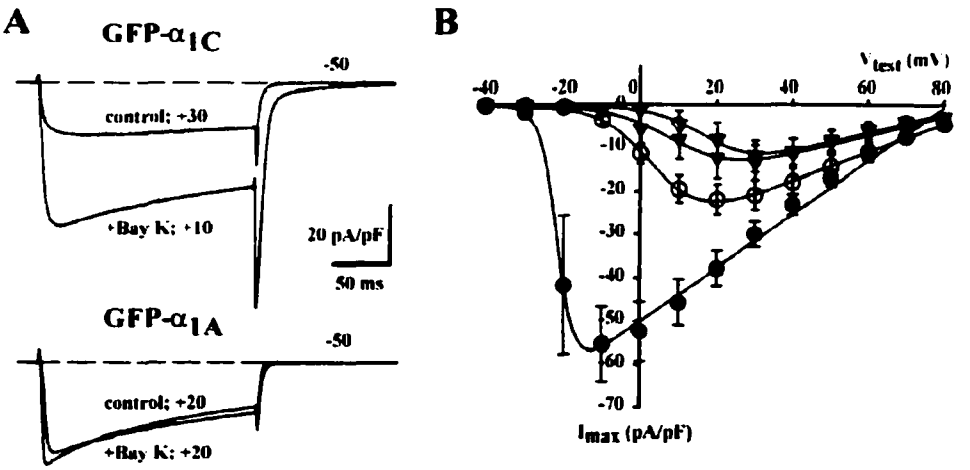

Figure 1.3. Dihydropyridine agonist potentiates GFP-α_{1C} but not GFP-α_{1A}. (A) Peak Ca^{2+} currents from GFP-α_{1C} (upper panel) or GFP-α_{1A} (lower panel) elicited by 200 ms depolarizations to the indicated test potentials in the absence (*control*) and presence (*+Bay K*) of 10 μM Bay K 8644. (B) Average current vs. voltage relationships for GFP-α_{1C} (circles; n = 5) and GFP-α_{1A} (inverted triangles; n = 7) in the absence (open symbols) or presence (filled symbols) of 10 μM Bay K 8644. The smooth curves represent best fits of equation (1) to the average data resulting in the values (*control* / *+Bay K*): GFP-α_{1C}, G_{max} = 337 nS/nF / 620 nS/nF, $V_{1/2}$ = 4 mV / -22 mV, V_{rev} = 93 mV / 81 mV, k_G = 7 mV / 2 mV; GFP-α_{1A}, G_{max} = 228 nS/nF / 225 nS/nF, $V_{1/2}$ = 18 mV / 11 mV, V_{rev} = 88 mV / 91 mV, k_G = 7 mV / 8 mV. [From Wilkens et al., 2001a.]

king maximal inward current for GFP-α_{1C}, together with a substantial increase in the magnitude of this current. In addition to affecting the peak current, Bay K 8644 also caused an approximately 3-fold increase in tail-current amplitude (I_{tail}) and in the time constant of tail-current deactivation (τ_{deact}) for GFP-α_{1C} (Fig. 1.3A, Table 1.1). Overall,

the effects of Bay K 8644 on GFP-α_{1C} tail currents qualitatively resemble those of strong depolarization (compare Figs. 1.2A and 1.3A).

TABLE 1.1

Parameters of DHP agonist- and depolarization-induced potentiation

	GFP-α_{1C}	GFP-α_{1C}(TQ→YM)	GFP-CACC	GFP-CCAA	GFP-α_{1A}
$I_{tail}^{+90} / I_{tail}^{+40}$	1.9 ± 0.3 (8)	2.5 ± 0.3 (11)	1.3 ± 0.1 (8)	1.1 ± 0.3 (7)	0.9 ± 0.1 (8)
$\tau_{deact}^{+90} / \tau_{deact}^{+40}$	2.6 ± 0.8 (5)	2.7 ± 0.3 (8)	1.2 ± 0.1 (8)	1.0 ± 0.1 (7)	0.9 ± 0.1 (6)
$I_{max}^{Bay\ K} / I_{max}^{control}$	2.7 ± 0.2 (5)	0.9 ± 0.1 (7)	3.4 ± 0.9 (5)	1.0 ± 0.1 (9)	1.1 ± 0.1 (7)
$V_{1/2}^{control} - V_{1/2}^{Bay\ K}$ (mV)	-24.9 ± 4.1 (5)	-3.3 ± 4.2 (6)	-15.7 ± 5.4 (5)	-3.0 ± 0.9 (9)	-3.9 ± 1.2 (6)
$I_{tail}^{Bay\ K} / I_{tail}^{control}$ (+40 mV)	3.3 ± 0.6 (5)	0.9 ± 0.1 (7)	6.2 ± 3.7 (5)	1.3 ± 0.4 (9)	1.2 ± 0.1 (6)
$\tau_{deact}^{Bay\ K} / \tau_{deact}^{control}$ (+40 mV)	2.9 ± 0.5 (5)	1.2 ± 0.1 (7)	3.0 ± 0.9 (5)	1.1 ± 0.1 (9)	1.2 ± 0.1 (6)

I_{tail} and τ_{deact} were determined as the amplitude (0.5 ms after repolarization) and time constant of decay (determined by fit of a single exponential) of tail currents produced by repolarization to -50 mV. Depolarization-induced potentiation was quantified as the ratios ($I_{tail}^{+90}/I_{tail}^{+40}$) or ($\tau_{deact}^{+90}/\tau_{deact}^{+40}$), where the superscripts indicate the test potential prior to repolarization. The effect of 10 μM Bay K 8644 was quantified in terms of four parameters: potentiation of peak currents ($I_{max}^{BayK}/I_{max}^{control}$), average shift in the voltage for half-maximal activation ($V_{1/2}^{BayK}$ - $V_{1/2}^{control}$), and potentiation of either I_{tail} ($I_{tail}^{BayK}/I_{tail}^{control}$) or τ_{deact} ($\tau_{deact}^{BayK}/\tau_{deact}^{control}$) after a test to +40 mV. All data are presented as mean ± SEM, with numbers in parentheses indicating the number of cells tested. [From Wilkens et al., 2001a.]

Figure 1.4 illustrates a more detailed characterization of tail currents in cells expressing GFP-α_{1C} or GFP-α_{1A}. Figure 1.4A shows the standard protocol for quantifying depolarization-induced potentiation, which was determined as the ratio of

either I_{tail} or τ_{deact} for a tail current following a V_{test} of +90 mV, to the corresponding values for a tail current following a V_{test} of +40 mV. By both measures, GFP-α_{1C} showed substantial depolarization-induced potentiation, whereas GFP-α_{1A} did not (Fig. 1.4A; Table 1.1). Figure 1.4B illustrates the dependence of I_{tail} on prior test potentials ranging from -40 to +80 mV. For GFP-α_{1A}, I_{tail} reached a maximum following a V_{test} of +30 mV,

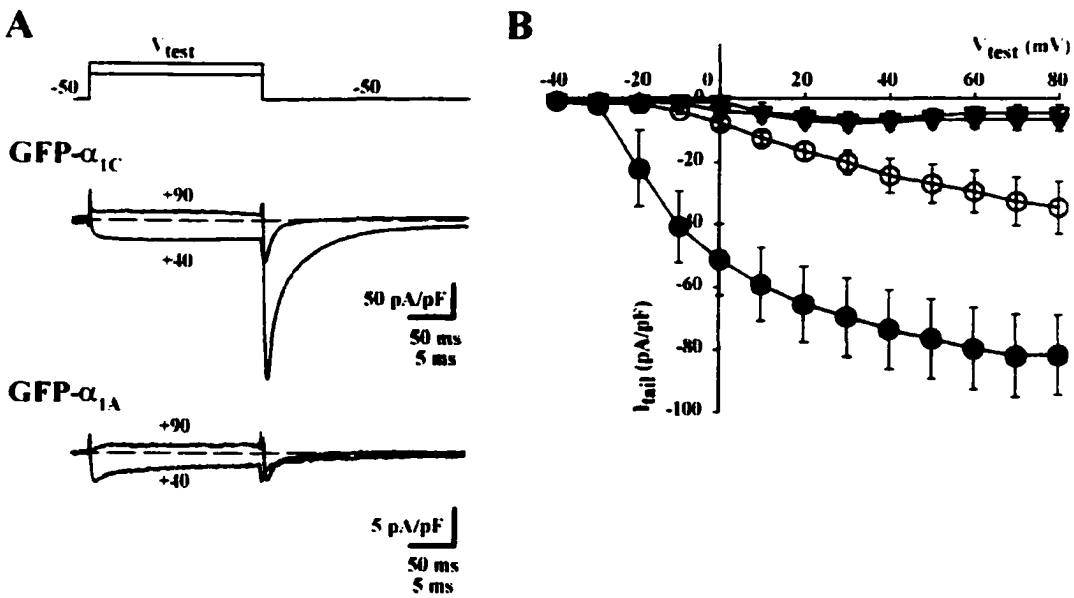

Figure 1.4. Strong depolarization induces potentiation of GFP-α_{1C} but not of GFP-α_{1A}. (A) Tail currents were elicited by depolarization from the holding potential (-80 mV) to -30 mV for 1s (to inactivate endogenous T-type current; Adams et al., 1990), a 30-50 ms repolarization to -50 mV, a 200 ms test depolarization (V_{test}) to varying potentials, followed by repolarization to -50 mV. Whole-cell currents are shown for GFP-α_{1C} (upper panel) and GFP-α_{1A} (lower panel) for test depolarizations of +40 and +90 mV. Note that for GFP-α_{1C}, the tail current following the V_{test} of +90 mV was larger and decayed more slowly than that after the V_{test} of +40 mV, whereas the tail currents for GFP-α_{1A} differed little for a V_{test} of +40 or +90 mV. The 50 ms time calibration applies to the currents during the test depolarization and the 5 ms calibration to the tail currents at -50 mV. (B) Relationship of tail-current amplitude (I_{tail}) at -50 mV to test pulse potential (V_{test}) for cells expressing GFP-α_{1C} (circles; n = 5) or GFP-α_{1A} (inverted triangles; n = 7) in the absence (open symbols) or presence (filled symbols) of 10 μM Bay K 8644. The amplitude of the tail currents for GFP-α_{1C} grew larger with increasing V_{test} over the entire range of potentials examined, while those for GFP-α_{1A} appeared to saturate with peak current. [From Wilkens et al., 2001a.]

in good agreement with the conductance vs. voltage curve calculated from peak currents (Fig. 1.2B). For still stronger depolarizations, I_{tail} became smaller for GFP-α_{1A}, as expected for a channel undergoing voltage dependent inactivation which becomes faster with stronger depolarization. In contrast to GFP-α_{1A}, I_{tail} for GFP-α_{1C} increased monotonically over the entire range of test potentials. This monotonic increase differs from the saturating conductance vs. voltage relationship (Fig. 1.2B) and is consistent with entry into a potentiated state having high P_o. This monotonic voltage dependence also suggests that depolarization-induced potentiation is not dependent upon Ca^{2+} entry during the prepulse. The application of 10 μM Bay K 8644 caused a still further increase in P_o. indicated by a substantial increase in I_{tail} for GFP-α_{1C} at any given test potential (Fig. 1.4B). In the presence of agonist, I_{tail} was still increased by stronger test depolarizations, up to at least +70 mV. Table 1.1 summarizes the effects of DHP agonist and strong depolarization on tail currents for GFP-α_{1C} and GFP-α_{1A}.

Mutation of T1066 and Q1070 of α_{1C} eliminates agonist- but not depolarization-induced potentiation

The observation that GFP-α_{1C} is potentiated by both agonist and strong depolarization, while GFP-α_{1A} is potentiated by neither, raises the possibility that agonist- and depolarization-induced potentiation are linked. As one test of this hypothesis, we created GFP-α_{1C}(TQ→YM), in which two residues of IIIS5 that are critical for the DHP sensitivity of α_{1C} (Mitterdorfer et al., 1996; He et al., 1997) were converted to the corresponding residues of α_{1A}. Currents produced by GFP-α_{1C}(TQ→YM) were not affected by the addition of 10 μM Bay K 8644 (Fig. 1.5A), whereas depolarization-

induced potentiation was intact (Fig. 1.5B). In particular, tail currents were larger and decayed more slowly following a V_{test} of +90 mV compared to a V_{test} of +40 mV (Fig. 1.5B, upper panel) and the tail-current amplitude increased monotonically as a function

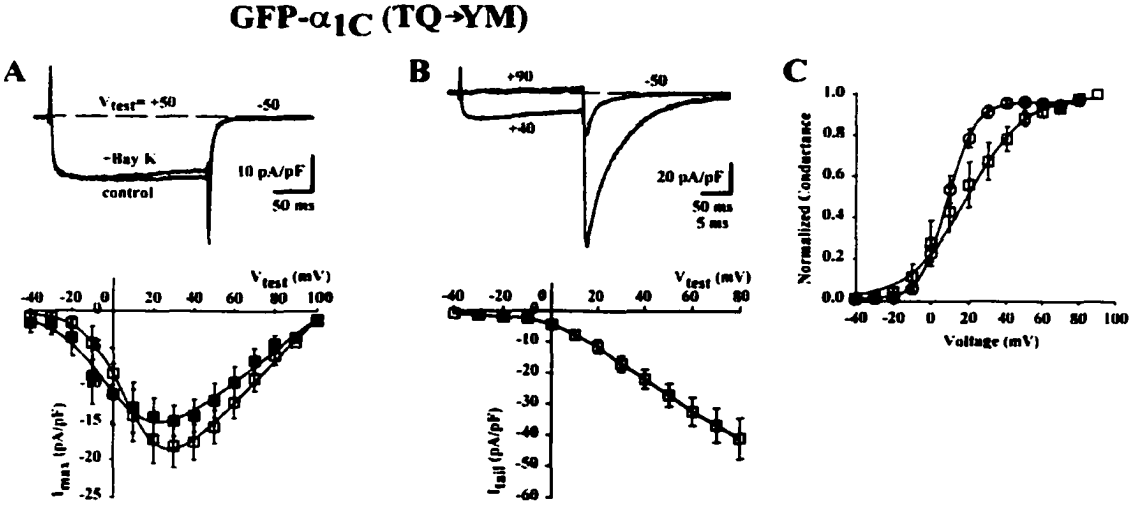

Figure 1.5. Mutation of the agonist binding site of GFP-α_{1C} abolishes potentiation by agonist (A) but not by depolarization (B). A, Upper panel: Whole-cell currents from a myotube expressing GFP-α_{1C}(TQ→YM) in the absence (*control*) or presence (+*Bay K*) of 10 μM Bay K 8644. *A*, lower panel: Average peak current vs. voltage relationship for GFP-α_{1C}(TQ→YM) in the absence (open squares; n = 7) or presence (filled squares; n = 7) of 10 μM Bay K 8644. The smooth curves represent best fits of the data with equation (1), yielding the values (*control* / +*Bay K*): G_{max} = 287 nS/nF / 218 nS/nF, $V_{1/2}$ = 9 mV / 1 mV, V_{rev} = 103 mV / 104 mV, k_G = 10 mV / 13 mV. *B*, Upper panel: Whole-cell currents for GFP-α_{1C}(TQ→YM) measured for test pulses to +40 or +90 mV, followed by repolarization to -50 mV; for clarity, the tail currents at -50 mV are shown on a faster time scale (5 ms calibration bar). *B*, Lower panel: Tail-current amplitudes at -50 mV as a function of prior test potential for GFP-α_{1C}(TQ→YM) (open squares; n = 11). (C) Conductance vs. voltage relationships for GFP-α_{1C} (circles; n = 9) and GFP-α_{1C}(TQ→YM) (squares; n = 10). The smooth lines represent best fits of the data with the expression: $1/\{1 + \exp[-(V-V_{1/2})/k_G]\}$, yielding the values: GFP-α_{1C}, $V_{1/2}$ = 9 mV, k_G = 7 mV; GFP-α_{1C}(TQ→YM), $V_{1/2}$ = 20 mV, k_G = 16 mV. [From Wilkens et al., 2001a.]

of test potential (Fig. 1.5B, lower panel). On average, GFP-α_{1C}(TQ→YM) was quantitatively similar to GFP-α_{1C} with respect to depolarization-induced potentiation, but was indistinguishable from GFP-α_{1A} in the lack of agonist-induced potentiation (Table 1.1). Interestingly, mutation of T1066 and Q1070 in the IIIS5 transmembrane segment of

α_{1C} resulted in a decreased steepness, and positive shift, of the steady-state activation curve in comparison to GFP-α_{1C} (Fig. 1.5C), indicating that these residues can affect activation gating. Taken together, the data of Figure 1.5 demonstrate that depolarization-induced potentiation still occurs in a mutant α_{1C} lacking a response to DHP agonist.

Agonist-induced potentiation persists in the absence of depolarization-induced potentiation

In an attempt to determine whether a single repeat of α_{1C} is sufficient to allow depolarization-induced potentiation, we constructed the chimeras GFP-CACC and GFP-CCAA and tested them for agonist- and depolarization-induced potentiation (Fig. 1.6). GFP-CACC consists of repeat II and the I-II linker of α_{1A} in an otherwise α_{1C} background (Fig. 1.6 A, C), and thus contains an intact DHP agonist binding site (Grabner et al., 1996; Hockerman et al., 1997; Ito et al., 1997; Sinnegger et al., 1997). As shown in Figure 1.6A, 10 μM Bay K 8644 potentiated maximum inward current in cells expressing GFP-CACC and caused a leftward shift in the peak current vs. voltage relationship. Quantitatively, both effects were similar to those of 10 μM Bay K 8644 on GFP-α_{1C} (Table 1.1). However, this chimera failed to show the large depolarization-induced potentiation characteristic of either GFP-α_{1C} or GFP-α_{1C}(TQ→YM) (Table 1.1; also, compare Fig. 1.6C with Figs. 1.5B and 1.4). Thus agonist-induced potentiation can be present in a channel construct that lacks significant depolarization-induced potentiation. The chimera GFP-CCAA (Fig. 1.6 B, D) consists of the first two repeats and the II-III linker of α_{1C} fused to repeats III and IV of α_{1A}. GFP-CCAA lacked both agonist- and depolarization-induced potentiation (Fig. 1.6B, D; Table 1.1).

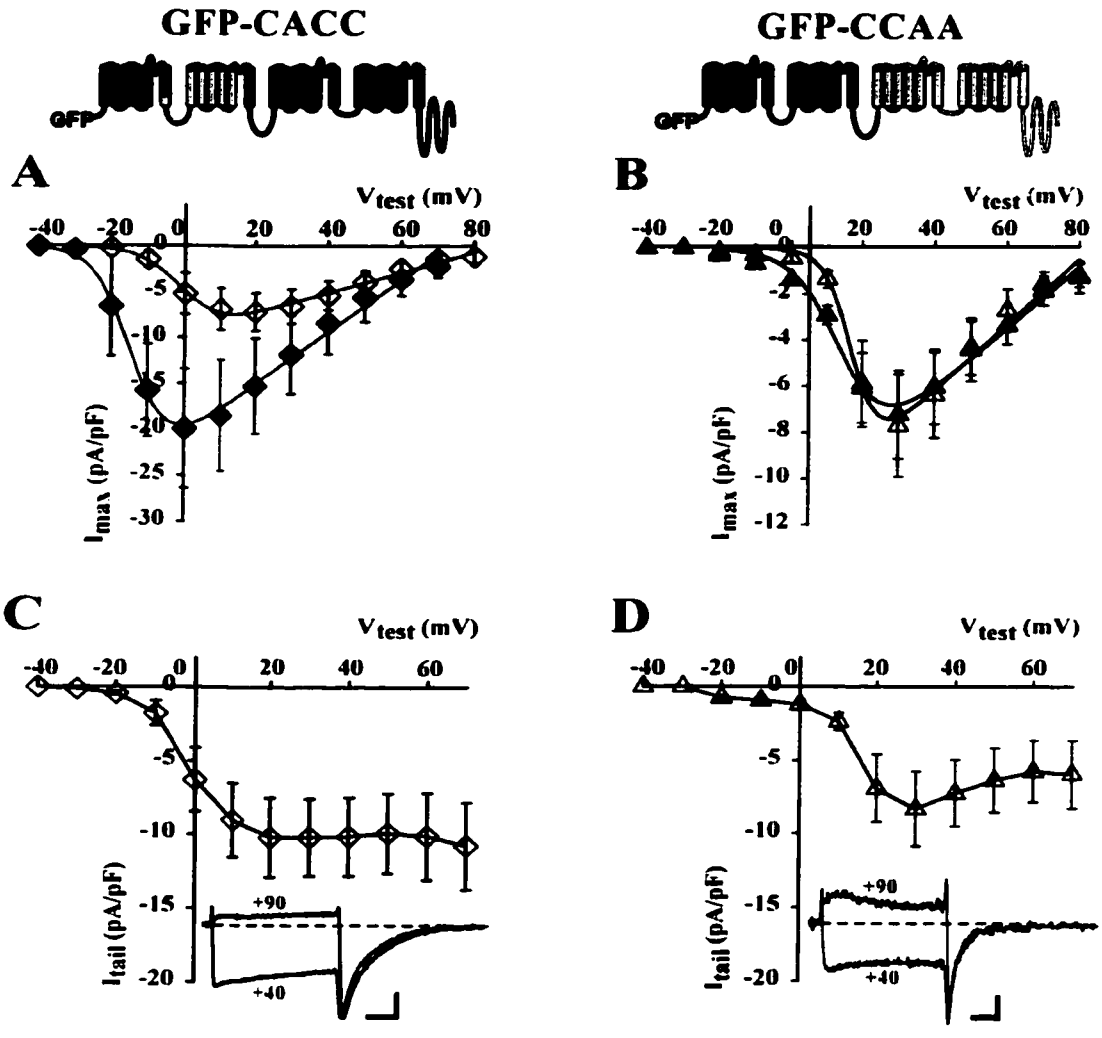

Figure 1.6. Presence or absence of potentiation by agonist or depolarization for chimeric channels. The chimeric channels GFP-CACC and GFP-CCAA are represented schematically with dark gray and light gray representing regions derived from α_{1C} and α_{1A}, respectively. (A, B) Average peak current vs. voltage relationships for cells expressing GFP-CACC (diamonds; n = 5) or GFP-CCAA (triangles; n = 7), in the absence (open symbols) or presence (filled symbols) of 10 μM Bay K 8644. The smooth lines represent best fits of equation (1) to the average data, yielding the values (*control / +Bay K*): GFP-CACC, G_{max} = 111 nS/nF / 283 nS/nF, $V_{1/2}$ = 0 mV / -14 mV, V_{rev} = 86 mV / 73 mV, k_G = 6 mV / 5 mV; GFP-CCAA, G_{max} = 142 nS/nF / 133 nS/nF, $V_{1/2}$ = 17 mV / 15 mV, V_{rev} = 84 mV / 86 mV, k_G = 4 mV / 7 mV. (C, D) Average values of tail-current amplitudes as a function of test potential for cells expressing GFP-CACC (open diamonds; n = 8) or GFP-CCAA (open triangles; n = 7). Insets illustrate superimposed currents elicited by test depolarizations to +90 or +40 mV, with the horizontal scale bars corresponding to 5 ms for the tail currents and 50 ms during the test depolarization. The vertical scale bars correspond to either 5 pA/pF (C) or 1 pA/pF (D). GFP-CACC was potentiated by agonist but not depolarization, while GFP-CCAA was potentiated by neither. [From Wilkens et al., 2001a.]

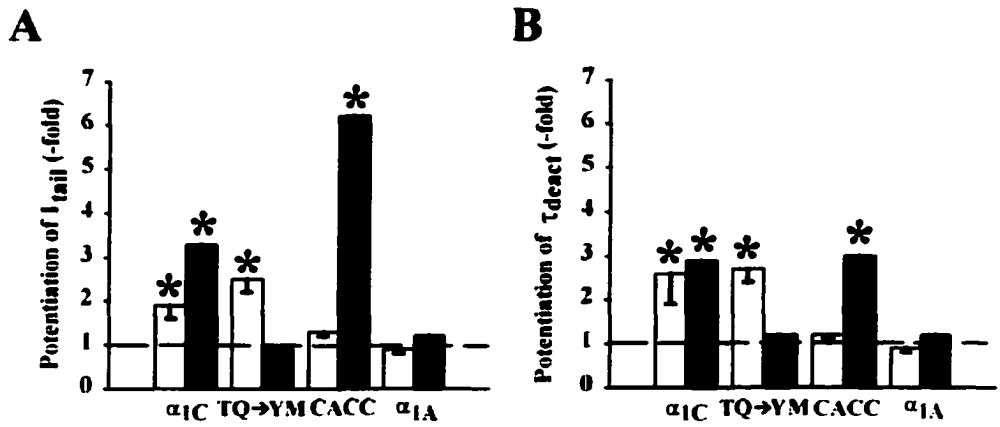

Figure 1.7. DHP agonist- and depolarization-induced potentiation occur via distinct mechanisms. (A) Average potentiation of tail-current amplitude by strong depolarization (I_{tail}^{+90} / I_{tail}^{+40}, white bars) or 10 μM Bay K 8644 (I_{tail}^{BayK} / $I_{tail}^{control}$, hatched bars) for the indicated constructs expressed in dysgenic myotubes. (B) Average potentiation of τ_{deact} by strong depolarization (τ_{deact}^{+90} / τ_{deact}^{+40}, white bars) or 10 μM Bay K 8644 (τ_{deact}^{BayK} / $\tau_{deact}^{control}$, hatched bars) for the indicated constructs expressed in dysgenic myotubes. The dashed lines at 1-fold indicate no potentiation. Asterisks indicate a significant difference ($p < 0.05$) from 1. The number of cells tested in each group ranged from 5 - 8. [From Wilkens et al., 2001a.]

Figure 1.7 summarizes the effects of strong depolarization and DHP agonist on the constructs GFP-α_{1C}, GFP-α_{1C}(TQ→YM), GFP-CACC and GFP-α_{1A}. The asterisks indicate a significant ($p < 0.05$) difference from 1-fold (where 1-fold indicates a lack of potentiation). Figure 1.7 demonstrates that depolarization-induced potentiation can persist in the absence of potentiation by agonist (i.e., GFP-α_{1C}(TQ→YM)), and potentiation by agonist can occur in the absence of depolarization-induced potentiation (i.e., GFP-CACC); therefore, the two processes likely occur via distinct mechanisms.

No single repeat of α_{1C} is sufficient for depolarization-induced potentiation

Figure 1.8 shows that in terms of both amplitude of I_{tail} (A) and τ_{deact} (B), the chimeras GFP-CACC and GFP-CCAA, like α_{1A}, lacked depolarization-induced

potentiation. Because GFP-CACC lacked depolarization-induced potentiation, none of the three cardiac repeats contained in this construct (I, III and IV) appears to be sufficient, individually or in concert, to mediate this process. In addition, because GFP-CCAA contains a cardiac repeat II and lacked depolarization-induced potentiation, a cardiac repeat II does not appear to be sufficient, either alone or in combination with repeat I. In conclusion, no single repeat of α_{1C} seems to be sufficient for depolarization-induced potentiation, which may instead represent a more global property. Several combinations of multiple repeats are tested by the chimeras examined in this paper, and others cannot be tested because not all possible combinations of repeats of L-type and non L-type sequence produce functional channels (Grabner et al., 1996; Spaetgens & Zamponi, 1999.)

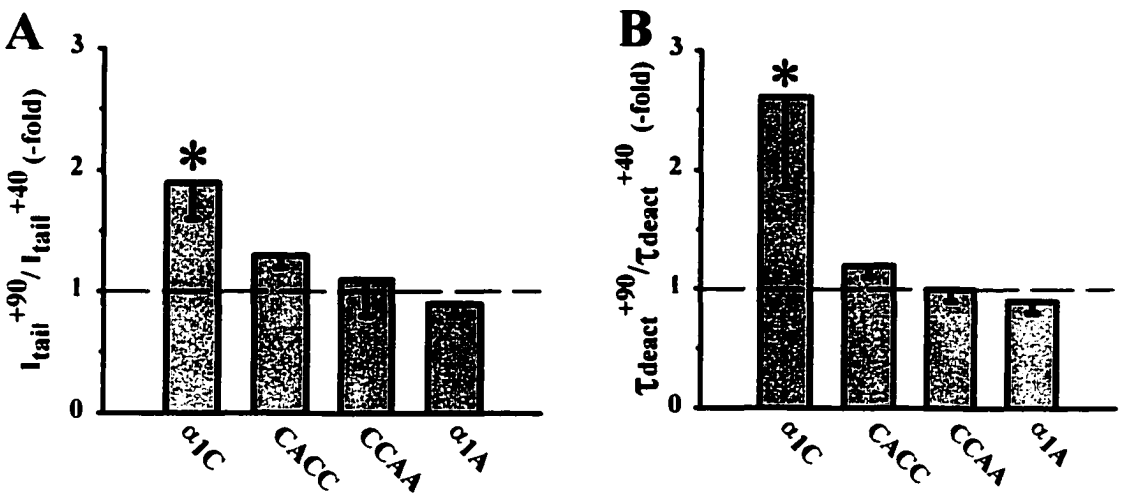

Figure 1.8. Depolarization-induced potentiation cannot be localized to any single channel repeat. Average depolarization-induced potentiation of tail-current amplitude (A), or tail-current deactivation (B) for the indicated constructs. The dashed lines at 1-fold indicate no potentiation. The number of cells tested in each group ranged from 5-8. Asterisks indicate a significant difference ($p< 0.05$) from 1. [From Wilkens et al., 2001a.]

Because potentiation is defined by a shift into a gating mode of substantially increased P_o, it seems likely that potentiation could not occur in a channel already having

a relatively high P_o. Therefore, it is of interest to know whether the lack of depolarization-induced potentiation in GFP-CACC and GFP-CCAA is a consequence of an already high P_o. We used equation (2) (see Methods) to estimate P_o for GFP-α_{1C}, GFP-CACC, GFP-CCAA and GFP-α_{1A} from measured values of G_{max} and Q_{max}. The values estimated by this approach for both GFP-α_{1C} and GFP-α_{1A} (Table 1.2) are in reasonable agreement with values determined from single channel measurements for α_{1C} (< 0.05, Cachelin et al., 1983; Lew et al., 1991) or α_{1A} (0.6, Llinas et al., 1989). Moreover, as shown in Figure 1.9, the estimated P_o for GFP-α_{1A} was about 30-fold higher than for GFP-α_{1C}. The estimated P_o for GFP-CCAA was similar to that of GFP-α_{1A}, but

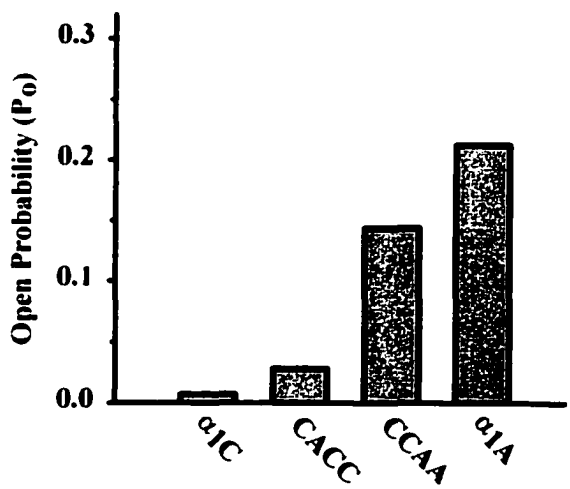

Figure 1.9. Low P_o is not a determinant of depolarization-induced potentiation. Channel open probability (P_o) was estimated according to equation (2) as described in the Methods. Values for Po were: α_{1C} = 0.01, CACC = 0.03, CCAA = 0.14, α_{1A}= 0.21. The number of cells tested in each group ranged from 5-8. [From Wilkens et al., 2001a.]

estimated P_o for GFP-CACC was much closer to that of GFP-α_{1C} (Fig 1.9; Table 1.2). The absence of depolarization-induced potentiation for GFP-CACC indicates that a low P_o alone is not a sufficient condition for this process to occur. The lack of depolarization-induced potentiation for GFP-CACC is even more striking given that this construct was strongly potentiated by agonist.

TABLE 1.2

Properties of wild-type and chimeric channels in dysgenic myotubes

	GFP-α_{1C}	GFP-CACC	GFP-CCAA	GFP-α_{1A}
I_{max} (pA/pF)	35.2 ± 4.1 (19)	7.0 ± 1.1 (16)	4.8 ± 1.1 (18)	22.3 ± 4.8 (16)
$V_{1/2}$ (mV)	+6.0 ± 0.6 (10)	+7.6 ± 2.2 (16)	+15.3 ± 1.5 (17)	−18.1 ± 1.7 (12)
G_{max} (nS/nF)	436.4 ± 76.1 (13)	118.5 ± 13.8 (16)	105.0 ± 20.7 (18)	352.0 ± 61.9 (16)
Q_{max} (nC/μF)	20.9 ± 2.7 (6)	3.0 ± 0.5 (11)	2.9 ± 0.4 (10)	3.2 ± 0.3 (7)
P_o	0.007 (5)	0.028 (6)	0.144 (6)	0.212 (7)

I_{max} is the peak inward current determined by measuring Ca^{2+} currents elicited with 200 ms test depolarizations ranging from –40 to +100 mV. Values for half-maximal activation potential ($V_{1/2}$) and maximal conductance (G_{max}) were determined by fitting peak Ca^{2+} currents according to equation (1). Maximum immobilization-resistant charge movement (Q_{max}) was measured by integration of the "On" gating current for a 15 ms step to +40 mV. Open channel probability (P_o) was estimated using equation (2) and measured values of $\overline{G_{max}}$ and $\overline{Q_{max}}$ as described in the Methods. All data are presented as mean ± SEM, with numbers in parentheses indicating the number of cells tested. [From Wilkens et al., 2001a.]

Discussion

In the present study, we have examined DHP- and depolarization-induced potentiation of L-type Ca^{2+} channels by expressing GFP-tagged cardiac (α_{1C}) and neuronal (α_{1A}) α_1 subunits in dysgenic myotubes. For GFP-α_{1C}, both strong depolarization and agonist (10 μM Bay K 8644) caused tail currents to become larger and to decay more slowly, whereas tail currents for GFP-α_{1A} were not affected by either

manipulation. Introduction of two point mutations (T1066Y and Q1070M) into GFP-α_{1C} abolished potentiation by agonist without any evident effect on potentiation by depolarization. Conversely, agonist but not depolarization caused potentiation of a chimera of α_{1C} and α_{1A} (GFP-CACC). Because depolarization-induced potentiation was absent for both GFP-CACC and the chimera GFP-CCAA, it appears that no single repeat of α_{1C} can be responsible for this process. GFP-CACC displayed a relatively low estimated P_o, quite similar to that of GFP-α_{1C}, while the estimated P_o for both GFP-CCAA and GFP-α_{1A} was much higher. Therefore, a channel which displays a low P_o (and is potentiated by agonist) can fail to be potentiated by depolarization.

Independent pathways for potentiation by DHP agonist and depolarization

Unitary records of L-type Ca^{2+} channels have been described as having three modes of gating upon depolarization: mode 0 (null sweeps), mode 1 characterized by brief openings (< 1 ms) in bursts, and mode 2 defined by longer openings and high P_o (Hess et al., 1984). Mode 1 is the predominant mode accessed during moderate depolarizations from the holding potential in the absence of DHP agonist, whereas mode 2 is promoted by the presence of agonist (Hess et al., 1984). Strong depolarization also promotes long openings of L-type channels in both chromaffin (Hoshi & Smith, 1987) and cardiac cells (Pietrobon & Hess, 1990). Because we have found that potentiation by either agonist or depolarization can be eliminated without a quantitative reduction in the effect of the other, it appears that these two processes occur via distinct pathways. In addition, we have used a concentration of agonist (10 μM Bay K 8644) which is supramaximal (Kokubun & Reuter, 1984); therefore, the additional potentiation of tail

currents by depolarization in the presence of the agonist also strongly suggests the presence of two independent pathways leading to a potentiated open state. Several other labs have likewise concluded from the additivity of the effects of depolarization and agonist, that these two stimuli cause an increased P_o by distinct pathways (Bourinet et al., 1994; Parri & Lansman, 1996). Moreover, single channel measurements show both different open times and first latencies depending on whether potentiation is induced by depolarization or agonist (Hoshi & Smith, 1987). In combination, these data suggest not only that mode 2 gating can be accessed by multiple pathways, but also that mode 2 consists of more than one potentiated open state.

Bay K 8644 is well known to shift activation in the hyperpolarizing direction (Hess et al., 1984; Sanguinetti et al., 1986; Fig. 1.3), indicating that it shifts equilibrium towards the open state of the channel. We have shown here that mutation of residues T1066 and Q1070 in the IIIS5 transmembrane domain of α_{1C} not only ablates the response to agonist but also shifts the voltage-dependence of activation oppositely, in the depolarizing direction. On this basis, one could hypothesize that Bay K 8644 promotes a conformation of these two residues that stabilizes open states of the channel, and mutation of these residues destabilizes this conformation.

Role of accessory subunits and of phosphorylation in depolarization-induced potentiation

The accessory β subunit has been shown to influence modal gating of α_{1C}. In particular, comparison of α_{1C} expressed with or without the β_{2a} subunit in *Xenopus* oocytes showed that β_{2a} increased both open times and the proportion of long openings (Costantin et al., 1998). β subunits have also been reported to affect depolarization-

induced facilitation, which may be mechanistically related to depolarization-induced potentiation (see Introduction). Specifically, depolarization-induced facilitation was found to occur when α_{1C} was co-expressed with the β_1, β_3 or β_4 subunits in *Xenopus* oocytes (Bourinet et al., 1994; Cens et al., 1998), but not with β_{2a} (Cens et al., 1996), raising the possibility that the β subunit plays a direct role in facilitation of α_{1C}, and perhaps in potentiation as well. However, others have found that depolarization-induced potentiation of the smooth muscle α_{1C} expressed in CHO cells occurs in the absence of any β subunit (Kleppisch et al., 1994). Whatever the exact role of the β subunit, our results demonstrate that potentiation is strongly influenced by the α_1 subunit itself, because all of the α_1 constructs examined in this study have a conserved "alpha interaction domain" (site of β subunit binding; Pragnell et al., 1994) and were expressed with a common β subunit (β_{1a}, which is endogenous to skeletal muscle; Ruth et al., 1989).

Evidence has been presented that PKA-dependent phosphorylation occurring during depolarizing prepulses is necessary for facilitation of α_{1S} in skeletal muscle cells (Sculptoreanu et al., 1993b; Johnson et al., 1994), the cardiac α_{1C} expressed in CHO cells (Sculptoreanu et al., 1993a) and the neuronal α_{1C} in dorsal root ganglia (Sculptoreanu et al., 1995). Evidence has also been presented that phosphorylation during depolarization is *not* involved in facilitation of the neuronal α_{1C} expressed in *Xenopus* oocytes, although basal phosphorylation may be required (Bourinet et al., 1994). If phosphorylation is required (either basal or voltage-dependent), then it seems unlikely to involve phosphorylation of α_{1C} directly because truncation of the consensus PKA sites (Gao et al., 1997) of the α_{1C} carboxyl tail does not eliminate facilitation (Cens et al., 1998).

Consistent with this result, we found that depolarization-induced potentiation does not occur for GFP-CACC even though it contains all the consensus PKA sites of α_{1C}.

Structural determinants of depolarization-induced potentiation and low P_o

As discussed above, brief openings predominate during activation of α_{1C} by modest depolarizations applied from a negative holding potential (mode 1 gating). The conformational changes responsible for activation of these brief openings occur rapidly (macroscopic activation occurs with a time constant of several ms at +30 mV; cf. Tanabe et al., 1991). Depolarization-induced entry into mode 2 occurs on a significantly slower time scale (with a time constant of several hundred ms at +30 mV) and over a much more positive voltage range (Pietrobon & Hess, 1990). Despite these differences, depolarization-induced potentiation resembles mode 1 activation in being strongly voltage dependent: based on two-state Boltzmann fits, the effective gating charge is 2.5 for depolarization-induced potentiation and 3.2 for mode 1 activation (Pietrobon & Hess, 1990). Thus, the question arises as to the identity of the voltage sensor for depolarization-induced potentiation. One possibility is that after undergoing the relatively rapid movements leading to mode 1 openings, the S4 segments can undergo subsequent, slower movements in response to still stronger depolarization. It is equally possible that structures other than S4 serve as voltage sensors for depolarization-induced potentiation. Because we found that neither GFP-CACC nor GFP-CCAA undergo depolarization-induced potentiation, it seems unlikely that the voltage sensing structures for depolarization-induced potentiation are localized within a single repeat. Rather,

depolarization-induced potentiation of α_{1C} appears to require large movements of charge distributed throughout the protein.

L-type channels like α_{1S} and α_{1C} differ from α_{1A} channels in that the L-type channels display agonist- and depolarization-induced potentiation, and also have a much lower P_o, raising the possibility that the structural determinants of potentiation and low P_o reside in similar structures. However, the chimera GFP-CACC had a relatively low P_o, yet did not display significant depolarization-induced potentiation. Because the chimera GFP-CCAA displayed a high P_o, the amino terminal half of α_{1C} (repeats I and II) does not appear to be an important determinant of low P_o; instead, structural requirements for low P_o may reside in the carboxyl half of the protein. Certainly, it is attractive to hypothesize that repeats III and IV are important for the intrinsic, low P_o of L-type channels since these same two repeats play an essential role in agonist binding, which increases P_o. A role for the carboxyl tail in determining P_o is suggested by previous work showing that P_o of α_{1C} is markedly increased by partial truncation of the carboxyl tail (Wei et al., 1994).

As stated earlier, the P_o of the L-type channels containing α_{1C} (< 0.05; Cachelin et al., 1983; Lew et al., 1991) is much lower than that of the neuronal channels containing α_{1A} (0.6, Llinas et al., 1989) or α_{1B} (0.5, Delcour & Tsien, 1993). Because single channel conductance varies less than 2-fold amongst these channels (α_{1C}: Kokobun & Reuter, 1984; α_{1A}: Zhang et al., 1993; α_{1B}: Rittenhouse & Hess, 1994), the production of an equivalent macroscopic current would require a much higher density of the L-type channels. A primary role of L-type Ca^{2+} channels in muscle is to regulate Ca^{2+} movements through ryanodine receptors. In order for this control to be relatively tight, it

may be useful to have an approximately 1-to-1 correspondence between the plasmalemmal L-type channels and the intracellular ryanodine receptors. Perhaps this correspondence is best served by a relatively high density of low P_o channels. Conversely, a high P_o and relatively low channel density would be advantageous when it is critical that a cellular response be triggered by the activation of only a few channels. Important goals for future work will be to better define the structures determining the differences in P_o between α_{1C} and neuronal channels like α_{1A} and α_{1B}, and to identify the conformational rearrangements that occur during potentiation of L-type channels.

CHAPTER 2

EXCITATION-CONTRACTION COUPLING IS UNAFFECTED BY DRASTIC ALTERATION OF THE SEQUENCE SURROUNDING RESIDUES L720-L764 OF THE α_{1S} II-III LOOP

Introduction

Excitation-contraction (EC) coupling depends upon the interaction of the voltage-gated L-type Ca^{2+} channel or dihydropyridine receptor (DHPR) of the plasma membrane and the intracellular Ca^{2+} release channel or ryanodine receptor (RyR) of the sarcoplasmic reticulum (SR). In contrast to cardiac muscle, EC coupling in skeletal muscle still occurs after blocking entry of L-type Ca^{2+} current; therefore, it is thought that membrane depolarization causes conformational changes of the skeletal DHPR (Schneider & Chandler, 1973; Rios & Brum, 1987) which in turn trigger the opening of the skeletal ryanodine receptor (RyR1) and the release of Ca^{2+} from SR stores (Fig. 2.1A). In addition to this orthograde EC coupling signal, a retrograde signal exists, by which RyR1 enhances L-type current through the DHPR (Nakai et al., 1996). Specifically, Ca^{2+} currents are small in dyspedic myotubes (which lack RyR1) despite

normal densities of the DHPR, while expression of recombinant RyR1 restores the L-type current density toward wild-type levels (Nakai et al., 1996).

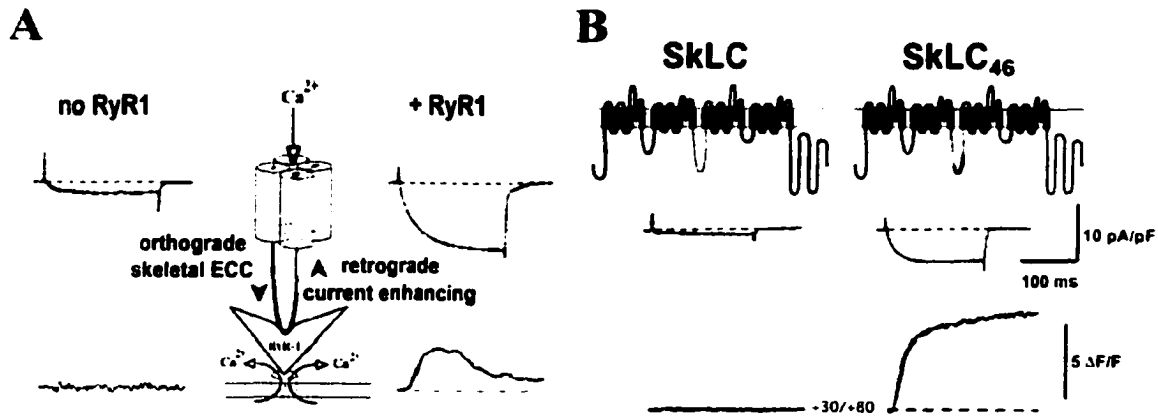

Figure 2.1. Bi-directional signaling in skeletal muscle. (A) Bi-directional signaling (center) consists of an orthograde EC coupling signal transmitted from the DHPR (α_{1S}) to RyR1 which results in intracellular Ca^{2+} release from the SR (Ca^{2+} transients, bottom row), and a retrograde signal transmitted from RyR1 to the DHPR, which enhances L-type Ca^{2+} current density (Ca^{2+} currents, top row). Cells lacking RyR1 do not support bi-directional signaling, as indicated by small Ca^{2+} currents and transients (left column), but expression of recombinant RyR1 in these cells restores large Ca^{2+} currents and transients (right column). (B) The cardiac II-III loop is unable to support orthograde or retrograde signaling in the skeletal/cardiac chimera SkLC (left). However, a 46 amino acid "critical domain" of the α_{1S} II-III loop inserted into the cardiac loop of SkLC is sufficient to restore bi-directional signaling in the chimera $SkLC_{46}$ (right). [Modified from Grabner et al., 1999.]

A fundamental goal for understanding the mechanism of bi-directional signaling is to identify the domains of the skeletal DHPR that directly participate in this process. One approach has been to analyze skeletal/cardiac chimeric DHPRs expressed in dysgenic myotubes, which lack the α_{1S} subunit of the skeletal DHPR (Chaudhari, 1992). Almost ten years ago, this work demonstrated that a cardiac DHPR containing the skeletal II-III loop was able to restore Ca^{2+}-entry independent (skeletal-type) EC coupling (Tanabe et al., 1990). A subsequent study identified 46 amino acids (residues 720-765) of the skeletal II-III loop which are sufficient for transferring strong, skeletal-type EC

coupling properties to an otherwise cardiac DHPR (Nakai et al., 1998). More recently, Grabner et al. (1999) showed that a skeletal DHPR with a cardiac II-III loop ("SkLC") lacked both orthograde (skeletal EC coupling) and retrograde (L-current enhancing) signaling (Fig. 2.1B, left). In particular, when α_{1S} residues 720-765, which had earlier been shown to confer skeletal-type coupling on an otherwise cardiac DHPR (Nakai et al., 1998), were introduced into SkLC, both skeletal-type EC coupling and wild-type Ca^{2+} current densities were restored (Fig. 2.1B, right). Thus, residues 720-765 of the skeletal DHPR II-III loop represent a "critical domain" for the bi-directional interaction between the skeletal DHPR and RyR1.

A limitation of chimeras is that they do not test the functional importance of regions that are conserved between the two parental proteins. This is a significant problem for the cardiac and skeletal DHPRs because the regions flanking the 46 residue critical domain are 56% identical between the cardiac and skeletal II-III loops. The potential importance of these flanking domains is emphasized by the results of experiments testing the effects of peptides on the function of RyR1 *in vitro* (ryanodine binding or Ca^{2+} release in SR vesicular preparations and open probability of RyRs reconstituted in artificial planar bilayers). In the earliest of these studies (Lu et al., 1994), recombinant peptides corresponding to either the skeletal or cardiac II-III loop were found to activate RyR1, which is difficult to reconcile with the results obtained with the chimeras (see above; Tanabe et al., 1990; Nakai et al., 1998; Grabner et al., 1999). Later, synthetic peptides (peptide A: α_{1S} residues 671-690; peptide As10: residues 681-690), which corresponded to smaller portions of the skeletal loop and were upstream from the critical domain identified in the chimera studies, were found to activate RyR1 (El-Hayek

et al., 1995; El-Hayek & Ikemoto, 1998; Dulhunty et al., 1999; Casarotto et al., 2000). In addition to the skeletal peptide (As10), the corresponding cardiac peptide (Ac10), which is homologous due to similar clusters of positively charged residues, was also found to cause activation of RyR1, although to a somewhat lower extent (Saiki et al., 1999). Similar cardiac peptides have also been reported not to cause activation of RyR1 (Zhu et al., 1999). Thus, the significance of the II-III loop regions flanking the critical domain remains uncertain.

Although the peptide experiments have the important advantage of providing a test of whether the skeletal DHPR and RyR1 interact directly, they have the disadvantage of lacking physiological context. In order to test the importance of the regions flanking the critical domain (L720-L764), including the As10 region, we examined chimeras constructed from mammalian (rabbit) skeletal DHPR and house fly (*Musca domestica*) DHPR (Grabner et al., 1994) sequence, which is highly divergent from both the skeletal and cardiac loops.

Materials and Methods

Construction of DHPR chimeras: DHPR II-III loop chimeras were constructed as follows, with asterisks indicating restriction sites introduced by polymerase chain reaction (PCR): **GFP-α_{1S}**: The cDNA coding sequence of the rabbit skeletal muscle DHPR α_{1S} subunit (Tanabe et al., 1987) was inserted in-frame 3' to the coding region of a green fluorescence protein (GFP) contained in a mammalian expression plasmid, as described previously (Grabner et al., 1998). **GFP-SkLM**: The EcoRI-BalI fragment of the rabbit skeletal muscle DHPR α_{1S} subunit (Sk) was coligated with the BalI-NdeI

fragment from the II-III loop (L) from the body wall muscle DHPR α_1 subunit (M) of *Musca domestica* (Grabner et al., 1994) into plasmid pSP72 (Promega) using the internal NdeI / EcoRI restriction sites. The same sites of pSP72 were also used to coligate two cDNA fragments, the NdeI* / XhoI fragment which was PCR generated from the clone GFP-SkLC (Grabner et al., 1999), plus the XhoI / BglII fragment of Sk. The PCR primer used to introduce the NdeI* site also mutated two amino acids of α_{1C} (A907, S908) to the corresponding Musca residues (G767, T768: see Fig. 1). The EcoRI / NdeI and NdeI* / BglII fragments were isolated from the two pSP72 subclones and coligated into the EcoRI / BglII cleaved pSP72 vector. Finally, the SalI / EcoRI fragment of Sk was coligated with the EcoRI / BglII fragment from the last pSP72 subclone into the SalI / BglII sites of GFP-α_{1S}. **GFP-SkLMS$_{45}$**: The MfeI / XbaI* fragment of M was coligated with the XbaI* / XhoI fragment of GFP-SkLM into the MfeI/XhoI sites of GFP-SkLM. Together with the XbaI* site, the 3' PCR primer introduced an upstream AflII* site, and the 5' primer introduced a ClaI* site downstream of the XbaI* cloning site. To yield plasmid GFP-SkLMS$_{45}$, an AflII* / TaqI* fragment of Sk was ligated into the AflII* / ClaI* sites of this subclone. All segments of cDNA generated and modified by PCR were checked by sequence analysis (MWG Biotech, Martinsried, Germany).

Expression of cDNA: The DHPR cDNAs were expressed in myotubes obtained as primary cultures from newborn dysgenic (*mdg/mdg*) mice (Adams & Beam, 1989) or myotubes produced by differentiation of the dysgenic cell line GLT (Powell et al., 1996). GLT cultures were transfected at the onset of myoblast fusion (2 to 4 days after addition of differentiation medium) using the liposomal transfection reagent FuGene according to the manufacturer's protocol (Roche). Primary dysgenic myotubes were microinjected

into a single nucleus (Tanabe et al., 1988) with solutions of DHPR cDNA (100-200 ng/μl) approximately one week after initial plating. Two to four days after transfection or injection, expressing myotubes were identified by GFP fluorescence and used in the experiments.

Electrophysiological characterization: Whole-cell patch clamp (Hamill et al., 1981) recording of Ca^{2+} currents and charge movements (Adams et al., 1990) was used to obtain an estimate of the ratio of maximum Ca^{2+} conductance to maximum immobilization-resistant charge movement (G_{max}/Q'_{max}), which provides a quantitative assessment of the strength of retrograde coupling. EC coupling was assayed in primary myotubes, as contractions in response to pulses (100 ms, 100 V) applied via an extracellular pipette (Tanabe et al., 1988), and in GLT myotubes, as fluorescence transients evoked in cells loaded with Fluo-4AM and stimulated with pulses (1 ms, 20-30 V) applied via electrodes placed on opposite sides of the culture dish (Flucher et al., 2000). To further assess EC coupling, depolarization-induced intracellular Ca^{2+} transients were measured microphotometrically during whole-cell recordings of primary myotubes by including tetrapotassium-Fluo-3 (Molecular Probes, Eugene, OR, USA) in the pipette solution (Garcia & Beam, 1994). All electrophysiological procedures, including test protocols, equipment, solutions and calculations were essentially the same as recently described for primary myotubes (Grabner et al., 1999) or GLT myotubes (Flucher et al., 2000) except that intracellular Ca^{2+} transients were recorded in the present study from primary myotubes expressing fluorescing GFP-tagged chimeras instead of coexpressing the CD8 reporter gene (Grabner et al., 1999).

Immunofluorescence Labeling: Differentiated GLT cultures expressing GFP-SkLM were fixed and immuno-stained as previously described (Flucher et al., 1994), using an affinity purified anti-GFP antibody (Molecular Probes, Eugene, OR, USA) at a dilution of 1:4,000 and the affinity purified antibody #162 against RyR1 at a dilution of 1:5,000 (Giannini et al., 1995). In double-labeling experiments, Alexa-conjugated secondary antibodies were used for GFP-SkLM, so that the antibody label and the intrinsic GFP signal were both recorded in the green channel, and Texas red-conjugated secondary antibodies were used for RyR1. Controls, such as the omission of primary antibodies and incubation with inappropriate antibodies, were routinely performed. Images were recorded on a Zeiss Axiophot microscope using a cooled CCD camera and MetaView image processing software (Universal Imaging, Corp., West Chester, PA, USA). At least three different experiments were performed for comparison of the wild-type DHPR (GFP-α_{1S}) and the DHPR chimera GFP-SkLM. Semi-quantitative evaluation of the labeling patterns (Flucher et al., 2000) revealed a clustering efficiency of greater than 50% in each experiment.

Results

An ancestral DHPR II-III loop as a tool to test DHPR-RyR1 interactions

Previous analysis of chimeric DHPRs constructed from skeletal and cardiac sequence showed that a "critical domain" of the α_{1S} II-III loop (residues L720-Q765) is required for both skeletal-type EC coupling (Nakai et al., 1998; Grabner et al., 1999) and RyR1-mediated enhancement of Ca^{2+} currents (Grabner et al., 1999). However, these experiments provided little or no information about the loop regions that flank the critical

domain because these regions are well conserved between the cardiac and skeletal proteins (Fig. 2.2B). In the present work we tested the importance of these flanking domains by replacing them with highly divergent sequences. To accomplish this, we created the chimera GFP-SkLM (Fig. 2.2A) in which the II-III loop of α_{1S} was replaced

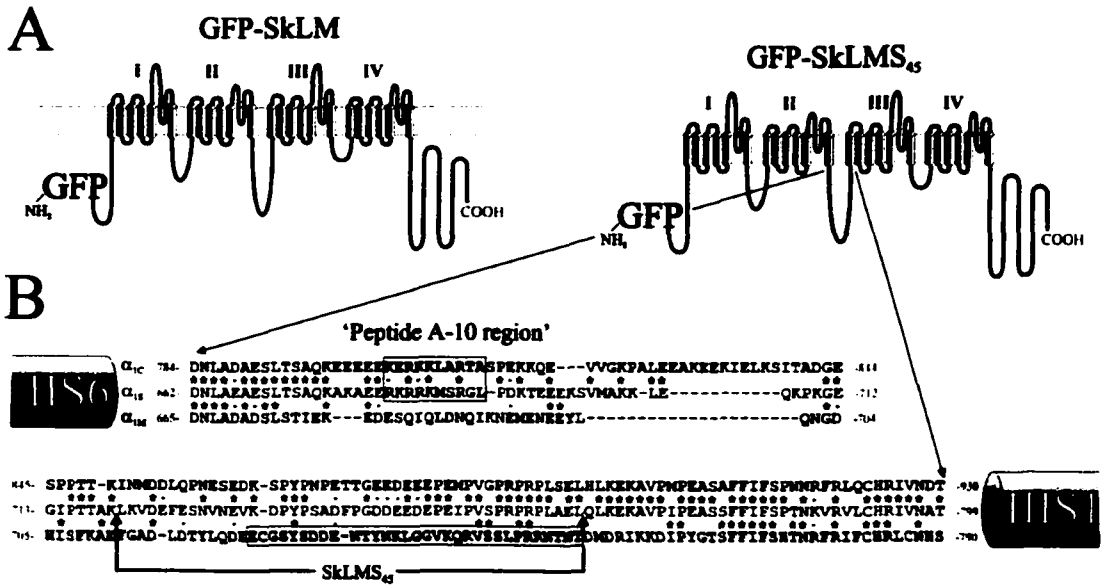

Figure 2.2. Schematic representation of the skeletal/*Musca* II-III loop DHPR chimeras, and II-III loop sequence alignments. (A) Rabbit skeletal muscle (α_{1S}) sequence is indicated in blue, and *Musca domestica* muscle (α_{1M}) is in black. (B) Alignment of cardiac (α_{1C}), skeletal (α_{1S}), and *Musca* (α_{1M}) II-III loop sequences. The *Musca* sequence boxed in gray (residues E724-T755) was replaced by the portion of α_{1S} sequence indicated by arrows (residues L720-L764) to yield GFP-SKLMS$_{45}$. Sequences boxed in yellow indicate the so-called skeletal and cardiac "peptide A-10 region" of EC coupling. Asterisks indicate amino acid identity, and dots show amino acids with identical charge. [From Wilkens et al., 2001b; drawn by M. Grabner.]

by the very divergent II-III loop of a DHPR cloned from the housefly (*Musca domestica*) (Grabner et al., 1994). Although we have not been able to express the *Musca* α_1 subunit functionally in various heterologous systems (Xenopus oocytes, tsA-201 cells or dysgenic myotubes), we did find that constructs containing parts of the *Musca* DHPR sequence were valuable for fine mapping of the DHP binding domain (Sinnegger et al.,

1997). The *Musca* II-III loop has comparable length (126 residues) to the cardiac and skeletal loops, but only 19% overall identity, most of which is concentrated at the two ends. Importantly, there is absolutely no homology to the peptide A-10 (As10/Ac10) region (Fig. 2.2B); this region has been suggested to be important in EC coupling because the isolated peptide activates RyR1 (El-Hayek et al., 1995; El-Hayek & Ikemoto, 1998; Dulhunty et al., 1999; Casarotto et al., 2000; Saiki et al., 1999). To test the role of the critical domain, we created the chimera GFP-SkLMS$_{45}$ (Fig. 2.2A) in which 32 residues (E724-T755) from the *Musca* loop of GFP-SkLM were replaced by α_{1S} residues L720-L764. In the absence of sequence homology that could serve as a guide post for the insertion of the α_{1S} critical domain into the *Musca* II-III loop, we chose to make this insertion within GFP-SkLMS$_{45}$ such that the critical domain was separated from IIS6 and from IIIS1 by the same number of residues as in wild-type α_{1S}. The final residue (Q765) of α_{1S} sequence previously tested in α_{1S} /α_{1C} chimeras (Nakai et al., 1998; Grabner et al., 1999) was omitted for cloning reasons.

The presence of α_{1S} residues 720-764 in the Musca II-III loop supports retrograde coupling

Expression of GFP-SkLM in dysgenic myotubes resulted in the presence of slowly activating (skeletal-type) Ca^{2+} currents, but these currents were much smaller than those for GFP-α_{1S} (Fig. 2.3A). To determine whether a reduced density of surface expression could account for the small Ca^{2+} currents produced by SkLM, we measured immobilization-resistant charge movements (Fig. 2.3B). The charge vs. voltage relationship was then fitted to determine the maximal charge movement (Q_{max}), as an

indirect measure of the expression density of DHPRs in the plasma membrane. Additionally, the current vs. voltage relationship for each cell was fitted (Adams et al., 1990) to yield a value of maximal Ca^{2+} conductance (G_{max}). For each of the constructs, GFP-α_{1S} and GFP-SkLM, neither G_{max} nor Q_{max} was found to differ significantly between

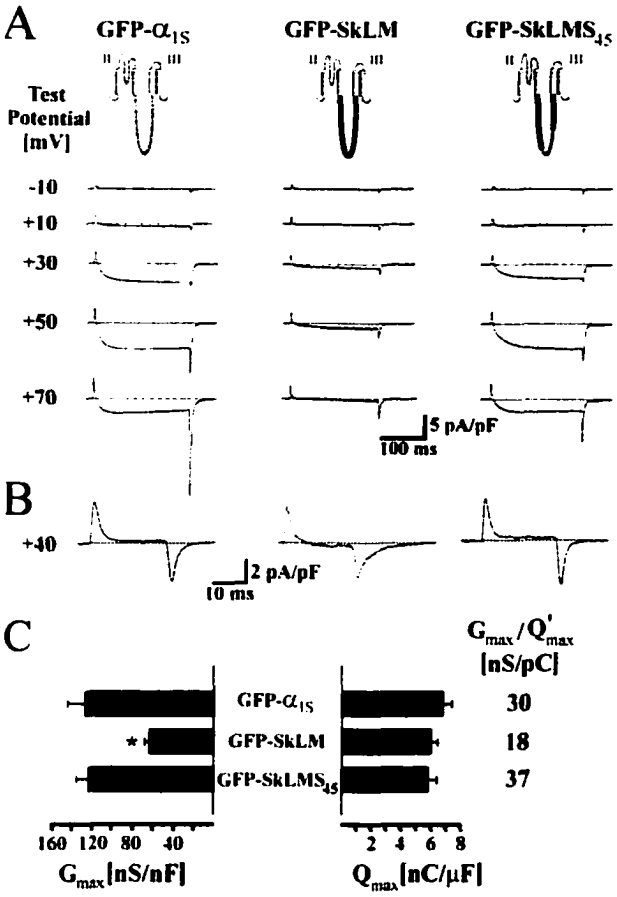

Figure 2.3. Restoration of retrograde coupling after insertion of α_{1S} residues 720-764 into the *Musca* II-III loop. (A) Representative whole-cell Ca^{2+} currents recorded from dysgenic myotubes expressing GFP-α_{1S} (left), GFP-SkLM (center), or GFP-SkLMS$_{45}$ (right). (B) Representative immobilization-resistant intramembrane charge movements measured at +40 mV for the same constructs indicated in (A). (C) Average maximal Ca^{2+} conductance (G_{max}, left) and charge movement (Q_{max}, right) and ratios of G_{max}/ Q'_{max} (center) for the same constructs. The asterisk indicates a significant ($p < 0.001$) difference in G_{max} from the other two constructs. No asterisk indicates lack of a statistically significant difference ($p > 0.1$). Bars represent the mean ± SEM of 12-20 recordings. [From Wilkens et al., 2001b; data collected by M. Grabner.]

injected primary dysgenic myotubes and transfected GLT myotubes (Table 2.1). Thus, data from the two types of dysgenic myotubes were combined for all subsequent analyses. As shown in Fig. 2.3C, the average G_{max} was significantly smaller for GFP-SkLM than for GFP-α_{1S}, whereas Q_{max} was similar for the two constructs. Because the Q_{max} values are similar, it appears that the *Musca* loop does not alter surface expression,

and that the reduction in current amplitude occurs because the *Musca* loop does not support retrograde signaling with the RyR1. Unlike GFP-SkLM, GFP-SkLMS$_{45}$ produced Ca^{2+} currents (Fig. 2.3A) similar in magnitude to those of GFP-α_{1S}. This similarity between GFP-SkLMS$_{45}$ and GFP-α_{1S} was also evident in the average values of

Table 2.1

Biophysical properties of channels expressed in dysgenic myotubes from primary culture or the GLT cell line

Construct	G_{max}, nS/nF	Q_{max}, nC/μF	G_{max}/Q'_{max}, nS/pC
GFP-α_{1S}	*154 ± 16 (15)*	*7.5 ± 0.8 (15)*	*31*
	127 ± 16 (13)	6.8 ± 0.5 (13)	30
GFP-SkLM	*60 ± 5 (14)*	*6.1 ± 0.4 (14)*	*17*
	67 ± 15 (6)	6.0 ± 1.4 (6)	19

Recordings from primary dysgenic myotubes are indicated in *italic* (top rows) and data from immortalized dysgenic GLT myotubes are indicated in roman (bottom rows). G_{max} is the maximal Ca^{2+} conductance calculated from peak currents, Q_{max} is the maximum charge movement integrated from the "On" gating current at +40 mV, and Q'_{max} is the difference between Q_{max} and the average, endogenous charge movement $Q_{dys(max)}$ found in dysgenic myotubes ($Q_{dys(max)}$=2.5 nC/μF; Adams et al., 1990). Brackets indicate a lack of significant difference ($p>0.05$). Data are given as mean ± SEM, where the numbers in parentheses indicate the number of cells tested. [From Wilkens et al., 2001b.]

G_{max} (Fig. 2.3C). Thus, the presence in the II-III loop of α_{1S} residues L720-L764, even when surrounded by sequence very unlike α_{1S}, was sufficient to restore the retrograde interaction whereby RyR1 increases the magnitude of slow L-type Ca^{2+} current.

The presence of α_{1S} residues 720-764 in the Musca II-III loop supports orthograde coupling

In GLT myotubes expressing GFP-α_{1S}, brief depolarizing pulses elicited transient elevations of intracellular Ca^{2+} which persisted even when Ca^{2+} influx was blocked by the

addition of Cd^{2+} and La^{3+} to the bath (Fig. 2.4A). By contrast, the addition of Cd^{2+} and La^{3+} abolished the depolarization-evoked Ca^{2+} transients in GLT myotubes expressing GFP-α_{1C}, although the SR was still capable of releasing Ca^{2+} in response to caffeine (Fig.

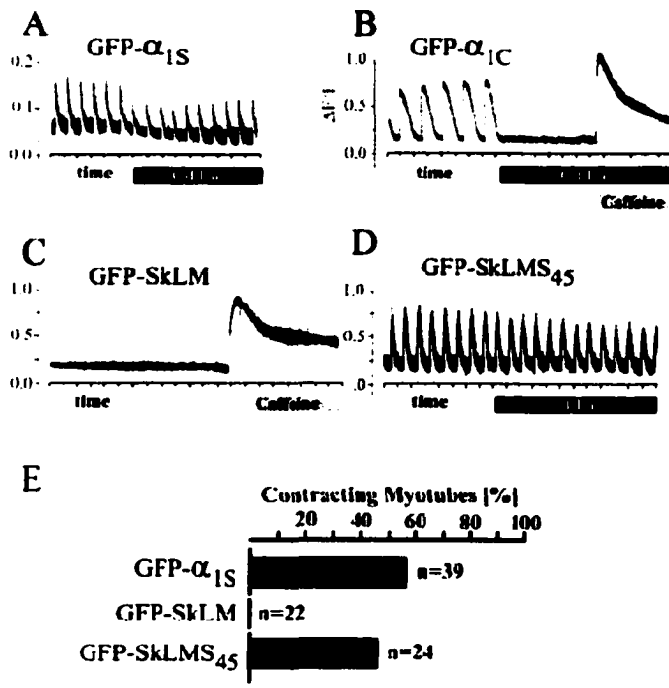

Figure 2.4. $SkLMS_{45}$ restores skeletal-type EC coupling after expression in dysgenic myotubes. (A-D) Action potential-evoked Ca^{2+} transients recorded from dysgenic myotubes expressing DHPR constructs, loaded with the fluorescent Ca^{2+} indicator Fluo-4 AM; tick marks on horizontal axis indicate 2s. GFP-α_{1S} (A) responded to 1 ms stimuli with Ca^{2+} transients that persisted after blocking currents with 0.5 mM Cd^{2+} and 0.1 mM La^{3+}, whereas the cardiac Ca^{2+} transients produced by GFP-α_{1C} (B) were abolished after blocking the DHPR with the Cd^{2+}/ La^{3+} solution. (C) GFP-SkLM failed to restore Ca^{2+} transients (n=10 dishes) even though Ca^{2+} release could be induced with 6 mM caffeine. GFP-$SkLMS_{45}$ (D) fully resored action potential-induced Ca^{2+} transients that were resistant to Cd^{2+}/ La^{3+} block of Ca^{2+} currents. (E) electrically evoked contractions (100 ms, 100V) recorded in Cd^{2+}/ La^{3+} from dysgenic myotubes expressing the indicated constructs, indicated as percentage of myotubes stimulated. [From Wilkens et al., 2001b.]

2.4B). Thus, GLT myotubes provide an appropriate system for distinguishing skeletal-type transients, which do not depend on entry of extracellular Ca^{2+}, from cardiac-type transients, which do depend upon such Ca^{2+} entry. Brief depolarizations failed entirely to evoke transients in GLT myotubes expressing GFP-SkLM, although the response to caffeine indicated that SR Ca^{2+} release was functional in these cells (Fig. 2.4C). By

contrast, skeletal-type transients were present in GLT myotubes expressing GFP-$SkLMS_{45}$ (Fig. 2.4D).

As a more quantitative measurement of the strength of EC coupling, we determined for each chimeric construct the fraction of injected primary myotubes which contracted in response to electrical stimulation in Cd^{2+}/La^{3+} solution. Contractions were never observed for GFP-SkLM, whereas the fraction of contracting myotubes was comparable for GFP-$SkLMS_{45}$ and GFP-α_{1S} (Fig. 2.4E). Like myotubes from normal

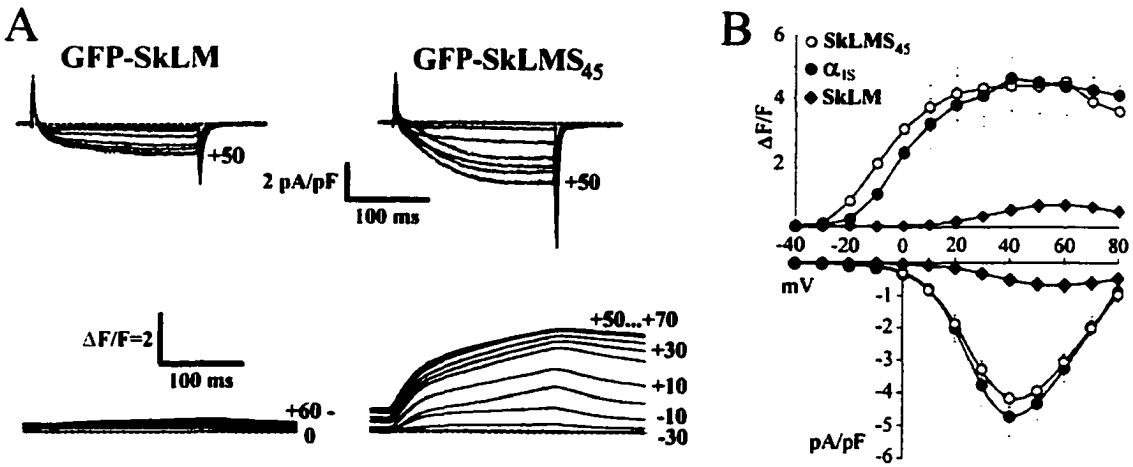

Figure 2.5. $SkLMS_{45}$ restores bi-directional signaling in dysgenic myotubes. (A) Whole-cell Ca^{2+} currents (upper panel) and depolarization-induced Ca^{2+} transients (lower panel) recorded simultaneously from dysgenic myotubes expressing GFP-SkLM or GFP-$SkLMS_{45}$. The vertical scale bar $\Delta F/F$ indicates Ca^{2+}-induced Fluo-3 fluorescence increments (ΔF) with respect to basal fluorescence (F). (B) Voltage dependence of Ca^{2+} transients ($\Delta F/F$; upper panel) and peak current densities (pA/pF; lower panel) recorded from dysgenic myotubes expressing GFP-α_{1S} (filled circles), GFP-SkLM (filled diamonds), and GFP-$SkLMS_{45}$ (open circles). Values represent the mean ± SEM of 11-20 recordings. [From Wilkens et al., 2001b.]

mice (data not shown), electrical stimulation failed to cause contraction of a fraction of dysgenic myotubes transfected with GFP-α_{1S} or GFP-$SkLMS_{45}$. These non-contracting

cells most likely represent myotubes in which components of the excitation-contraction coupling machinery are not fully developed (see Flucher et al., 2000).

In addition to examining EC coupling in intact myotubes, we also used whole-cell patch clamping to characterize the voltage dependence of Ca^{2+} release in primary dysgenic myotubes expressing GFP-α_{1S}, GFP-SkLM and GFP-SkLMS$_{45}$. Very small Ca^{2+} transients were present for GFP-SkLM (Fig. 2.5A). Moreover, these transients appeared to depend upon Ca^{2+} entry because the amplitude of the transient had a voltage dependence mirroring that of Ca^{2+} current (Fig. 2.5B). Additionally, the Ca^{2+} transients for GFP-SkLM were blocked by the addition of Cd^{2+} and La^{3+} to the bath (data not shown). In myotubes expressing GFP-SkLMS$_{45}$, the Ca^{2+} transients were large (Fig. 2.5A), and did not differ significantly in either magnitude or voltage dependence from those of GFP-α_{1S} (Fig. 2.5B). Thus, placing α_{1S} residues L720-L764 into the very dissimilar background of the *Musca* II-III loop was able to restore both orthograde and retrograde coupling with RyR1.

A prerequisite for the bi-directional interaction between a DHPR construct and RyR1 is the colocalization of the two proteins in junctions between the plasma membrane and SR. If GFP-SkLM were not targeted into junctions, this could explain the absence of bi-directional signaling observed for this construct. Fig. 2.6 compares the subcellular distribution of GFP-SkLM (top panel) with that of RyR1 (middle panel). Both proteins are present in discrete clusters that overlap with one another and clusters were observed in 54% of transfected myotubes (n=200), which is close to the value observed in GFP-α_{1S} transfected myotubes (58%; n=967). This colocalization, which indicates correct junctional targeting, is particularly evident in the pseudo-color overlay image (bottom)

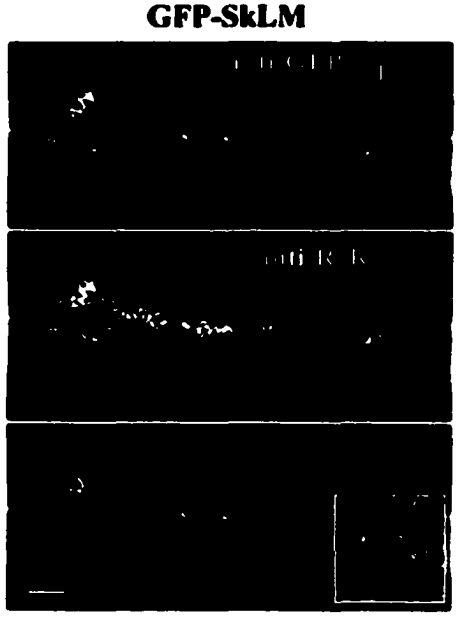

Figure 2.6. Failure of GFP-SkLM to restore bi-directional signaling is not due to a lack of correct junctional targeting. Subcellular localization of GFP-SkLM in a transiently transfected GLT myotube. Double immunofluorescence labeling was performed with antibodies against GFP, N-terminally fused to SkLM (top), and against RyR1 (middle). The merged image (bottom) illustrates the colocalization (yellow) of GFP-SkLM (green) and RyR1 (red) in discrete clusters which represent junctions of the SR with transverse tubules or with the plasma membrane. Arrows indicate examples of colocalization. *Inset* shows a 2-fold enlarged view of co-clustered channels. N, nuclei. Bar = 10 μm. [From Wilkens et al., 2001b; data collected by B. Flucher.]

in which green and red indicate GFP-SkLM and RyR1, respectively, and yellow shows sites of colocalization. Because GFP-SkLM is able to target to junctions between the plasma membrane and SR, and because its targeting is not different from that of GFP-SkLMS$_{45}$ (clusters found in 58% of transfected myotubes (n=65; micrograph not shown), a failure to colocalize cannot account for the lack of bi-directional signaling by GFP-SkLM.

Discussion

EC coupling in skeletal muscle likely involves allosteric coupling between α_{1S} and RyR1, either by direct contact between the two proteins or by way of intervening proteins. Using chimeras based on the II-III loop of the *Musca* DHPR, we have shown that residues L720-L764 of α_{1S} contain a critical domain which is essential for both EC

coupling and retrograde signaling. This result is in agreement with previous work using chimeras based on the II-III loop of α_{1C} (Nakai et al., 1998; Grabner et al., 1999). The new finding that bi-directional signaling survives a drastic change in the sequence of the As10 region makes it very unlikely that this region plays an important role in the activation of RyR1 during EC coupling as previously postulated (El-Hayek & Ikemoto, 1998; Dulhunty et al., 1999; Zhu et al., 1999). A similar conclusion was also reached on the basis of a skeletal DHPR in which only the As10 region was scrambled (Proenza et al., 2000).

A model of allosteric coupling between α_{1S} and RyR1 would appear to have two requirements. First, there must be anchoring interactions that maintain α_{1S} and RyR1 in a precise spatial coordination with respect to one another. Second, the allosteric coupling between α_{1S} and RyR1 during orthograde signaling must involve one or more cytoplasmic domains of α_{1S} that undergo conformational changes in response to movement of the voltage sensing domains. Thus, the critical domain of the II-III loop could be involved in protein-protein interactions that were either static (anchoring) or dynamic (undergoing conformational changes during orthograde signaling) or both. If the critical domain plays a dynamic role in EC coupling, then conformational changes are unlikely to be transmitted to it via the peptide backbone since signaling is normal after large changes in the sequence of the flanking regions. Whatever the role of the critical domain, the important result of the present work is that bi-directional signaling is not affected by dramatic changes in the primary sequence of the loop regions which flank the critical domain. Thus, these flanking regions are unlikely to be sites of protein-protein interaction necessary for bi-directional signaling.

CHAPTER 3

A ROLE FOR THE CARBOXYL TERMINAL OF THE SKELETAL DHPR (α_{1S}) IN CHANNEL BIOSYNTHESIS AND TARGETING IN SKELETAL MUSCLE

Introduction

The functional interaction between DHPRs and RyRs occurs at specialized junctions between the sarcolemmal and sarcoplasmic reticulum membranes and thus requires that both proteins be targeted to and anchored at the junctions. However, the mechanisms for targeting and anchoring are poorly understood. Although the two proteins may interact with one another directly, other molecular interactions must also be involved because RyRs target to junctions in dysgenic muscle cells (Powell et al., 1996) lacking DHPRs (Knudson et al., 1989), and DHPRs target to junctions in dyspedic muscle cells, which lack RyRs (Takekura et al., 1995; Takekura et al., 1999).

The targeting of the DHPR seems likely to depend upon structures within the α_{1S} subunit, because GFP-tagged α_1 subunits show a very different subcellular distribution in dysgenic myotubes depending on whether they are the neuronal or muscle type (Grabner et al., 1998). The carboxyl tail of several members of the voltage-gated ion channel superfamily such as Shaker potassium (Kim et al., 1995), sodium (Gee et al., 1998), and

Trp Ca^{2+} channels (Shieh et al., 1996) appears to play a role in channel localization, often via interactions with other cellular proteins. Specific evidence for the involvement of the α_{1S} carboxyl tail in targeting was presented recently by our lab (Proenza et al., 2000). In this study, we examined α_{1S} channels that were truncated or mutated, demonstrating that when a 120 residue domain of the C-terminus ("target"; residues 1543-1662) was removed or mutated, channel expression and targeting to the triad junction were severely disrupted. However, as summarized in Figure 3.1, although Ca^{2+} conductance and charge

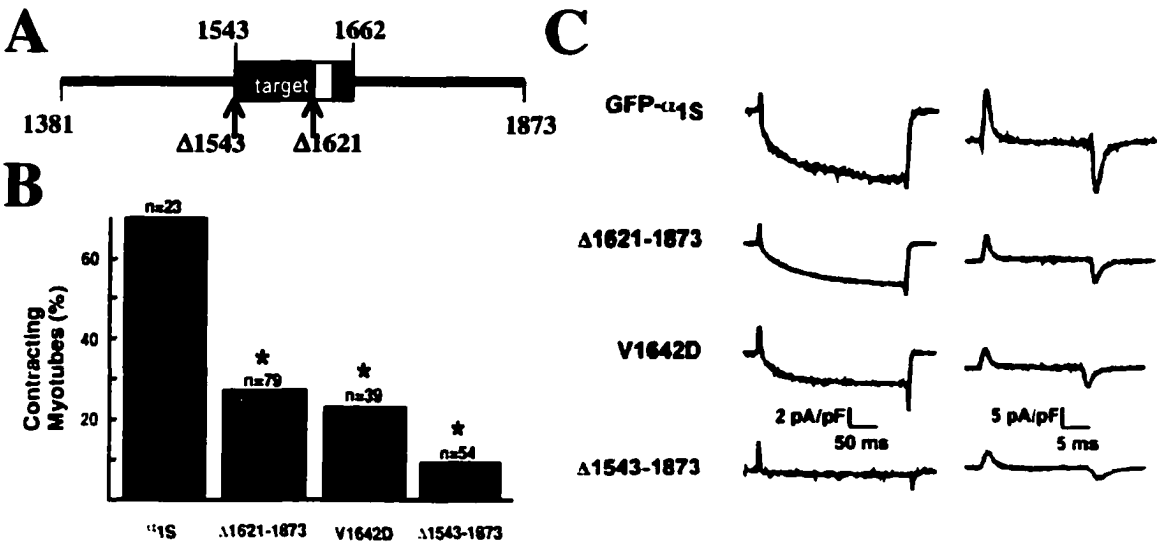

Figure 3.1. Residues 1543-1662 of α_{1S} play a role in channel biosynthesis. (A) Schematic representation of the α_{1S} C-terminus (residues 1381-1873), where the black box indicates a 120 residue domain called "target" (residues 1543-1662), the white box indicates a putative PDZ binding motif (residues 1640-1642), and the two arrows indicate sites of truncation for the α_{1S} constructs Δ1543-1873 and Δ1621-1873. Thus, Δ1543-1873 lacked "target", Δ1621-1873 contained 75 residues of "target" but lacked the PDZ binding motif, and V1642D contained a single point mutation within the PDZ motif of an otherwise intact C-terminus. (B) Percentage of contracting myotubes in response to electrical stimulation (10 ms/100 V) for the indicated constructs. (C) Ca^{2+} currents (left) and charge movements (right) for the indicated constructs following expression in dysgenic myotubes. Removal or mutation of "target" severely reduced Ca^{2+} currents, charge movements and contractility of myotubes expressing truncated or mutated channels, supporting a role for residues 1543-1662 in channel expression. [Modified from Proenza et al., 2000.]

movements were significantly reduced after truncation or mutation of "target," some functional protein was still expressed at the membrane and targeted correctly to junctions (indicated by Ca^{2+} currents, charge movement, and restored electrically evoked contractions of dysgenic myotubes expressing α_{1S} constructs). The subsequent work of Flucher et al. (2000) showed that a neuronal channel (α_{1A}) which is not normally targeted to junctions, can be targeted correctly ~28-47% of the time if either the entire carboxyl tail of α_{1S}, or a 55 residue portion of the carboxyl tail, are inserted into the carboxyl tail of α_{1A}. However, the restored junctional targeting of either of these two chimeric channels never reached the efficiency of the wild-type α_{1S} (58%). Taken together, these data support the idea that other regions of α_{1S} outside of "target" must be involved in targeting and/or biosynthesis of the α_{1S} protein.

In order to determine whether "target" alone is sufficient for the expression and targeting of α_{1S}, we constructed a GFP-tagged chimeric channel (GFP-α_{1H}+target), containing α_{1S} "target" fused at the C-terminus of a highly divergent T-type Ca^{2+} channel, α_{1H}. α_{1H} is only about 15% conserved with α_{1S} and contains none of the EF hand (Ca^{2+} binding), IQ (calmodulin binding), or AID (site of β subunit binding) regulatory domains which could participate in channel targeting or biosynthesis. We expressed cDNAs encoding wild-type or chimeric channels in dysgenic myotubes to examine whether the presence of "target" could alter expression or targeting of α_{1H}.

Materials and Methods

Construction of cDNAs: PCR = polymerase chain reaction, nt = nucleotide(s), and bp = base pair(s). The wild-type construct pCDNA-α_{1H} was constructed by inserting the α_{1H}

coding sequence (kindly provided by Dr. T.P. Snutch in a pBluescript plasmid) into the HindIII / XbaI restriction sites of the mammalian expression vector pCDNA 3.0. The N-terminal GFP fusion protein (GFP-α_{1H}) was created by introducing a unique 5' SalI* restriction site at nt -18 of the α_{1H} coding sequence (where nt 1 represents the A of the initiating Methionine), and ligating the SalI* / XbaI (nt 1-7575) fragment of α_{1H} into the corresponding restriction sites of a modified CMV-GFP expression vector (Grabner et al., 1998). The chimeric channel GFP-α_{1H}+target consisted of residues 1543-1662 of α_{1S} fused 162 residues downstream of IVS6 to GFP-α_{1H} (exactly as "target" is positioned in the wild-type α_{1S}). To construct GFP-α_{1H}+target, the SphI / BamHI fragment of GFP-α_{1H} (nt 6902-9267) was subcloned into the corresponding restriction sites of pSP64 (Promega) to create the subclone p64+H. The Quickchange mutagenesis kit (Stratagene) was used to introduce a unique SalI* site (silent) into p64+H (at nt 7756 of GFP-α_{1H}), thus yielding p64+H/SalI*. Three rounds of overlapping PCR using GFP-α_{1H} or GFP-α_{1S} (Grabner et al., 1998) as template were used to amplify a chimeric product encoding "target" (α_{1S} residues 1543-1662 followed by a stop codon) flanked by 5' and 3' sequences from GFP-α_{1H} (5' nt 7752-7770, introducing SalI* at nt 7756, and 3' nt 9370-9900, introducing BamHI* at nt 9892). Following digestion with SalI and BamHI, the PCR product was subcloned into p64+H/SalI*, and the final BstEII / BsmI fragment from that subclone (nt 7566-9391 of GFP-α_{1H} containing "target") was ligated into the corresponding restriction sites of GFP-α_{1H}. All sequences obtained using PCR were sequenced to ensure accuracy (Macromolecular Resources, Fort Collins, CO).

Expression and Electrophysiological Analysis of Channels in Dysgenic Myotubes: One week after plating, primary cultures of mouse dysgenic myotubes (Adams et al., 1989),

which lack an endogenous α_{1S} subunit (Knudson et al., 1989), were microinjected in single nuclei with cDNAs (100 ng/μl) encoding α_1 subunits. pCDNA-α_{1H} was coinjected with GFP (10 ng/μl). Myotubes were examined either 24 hours or 48 hours after injection (ranges: 24-27 hours, and 48-52 hours) for green fluorescence and used for electrophysiological analysis. Macroscopic Ca^{2+} currents were measured using the whole-cell patch clamp method (Hamill et al., 1981). Whole-cell patch pipettes of borosilicate glass had resistances of 1.5-2.0 MΩ when filled with an internal solution containing 140 mM Cs-aspartate, 10 mM Cs_2EGTA, 5 mM $MgCl_2$, and 10 mM HEPES (pH 7.4 with CsOH). The external bath solution contained 10 mM $CaCl_2$, 145 mM TEA-Cl, and 10 mM HEPES (pH 7.4 with TEA-OH), plus 3 μM tetrodotoxin. Test currents were obtained by stepping from a holding potential of –80 mV to variable test potentials, and repolarizing to –80 mV. Occasionally whole-cell currents were recorded stepping from –50 mV, which did not affect the amplitude of peak currents (data not shown). Test currents were corrected for linear components of leak and capacitative currents by digitally scaling and subtracting the average of ten preceding control currents elicited by hyperpolarizing steps (20-40 mV in amplitude) applied from the holding potential. Data were sampled at 1 kHz, and were included only for cells in which the maximum voltage error (calculated by the product of peak inward current and compensated series resistance) was < 10 mV. Maximal Ca^{2+} conductance (G_{max}) and half-maximal activation potential ($V_{1/2}$) were calculated by fitting peak inward current values for each cell with the equation:

$$I = G_{max} * (V-V_{rev}) / \{1 + \exp [-(V-V_{1/2}) / k_G]\} \quad (1)$$

where I is the peak inward Ca^{2+} current measured at the test potential (V), V_{rev} is the reversal potential, and k_G is a slope factor.

Statistical Analysis: Statistical significance was assessed using one-way analysis of variance (ANOVA) using α=0.05, and SAS software (Version 8). All data are presented as mean +/- S.E.M.

Results

The GFP tag does not alter the functional properties of α_{1H}

Figure 3.2A illustrates the T-type Ca^{2+} channel constructs examined in this study. pCDNA-α_{1H} consisted of the T-type channel α_{1H} contained in a mammalian expression vector, GFP-α_{1H} was constructed by fusing GFP to the N-terminus of α_{1H}, and GFP-α_{1H}+target contained residues 1543-1662 of α_{1S} ("target") fused to GFP-α_{1H} 162 residues downstream of IVS6 (exactly as "target" is positioned in the wild-type α_{1S}).

Figure 3.2B illustrates representative whole-cell family currents for native T-type channels as well as cloned channel constructs 24 hours after expression in dysgenic myotubes. Ca^{2+} currents showed the rapid activation and inactivation, and slow deactivation kinetics typical of T-type channels. Average, peak current voltage-relationships for native and cloned channels are shown in Figure 3.2C. Native T-type currents ranged from 0-17 pA/pF, averaging ~5 pA/pF. Currents produced by pCDNA-α_{1H}, GFP-α_{1H}, and GFP-α_{1H}+target were ~5-fold larger, on average. 24 hours after expression, steady state activation parameters (Table 3.1) and peak curent densities for pCDNA-α_{1H} and GFP-α_{1H} were indistinguishable ($p > 0.1$), indicating that the GFP tag did not alter the functional properties of α_{1H}.

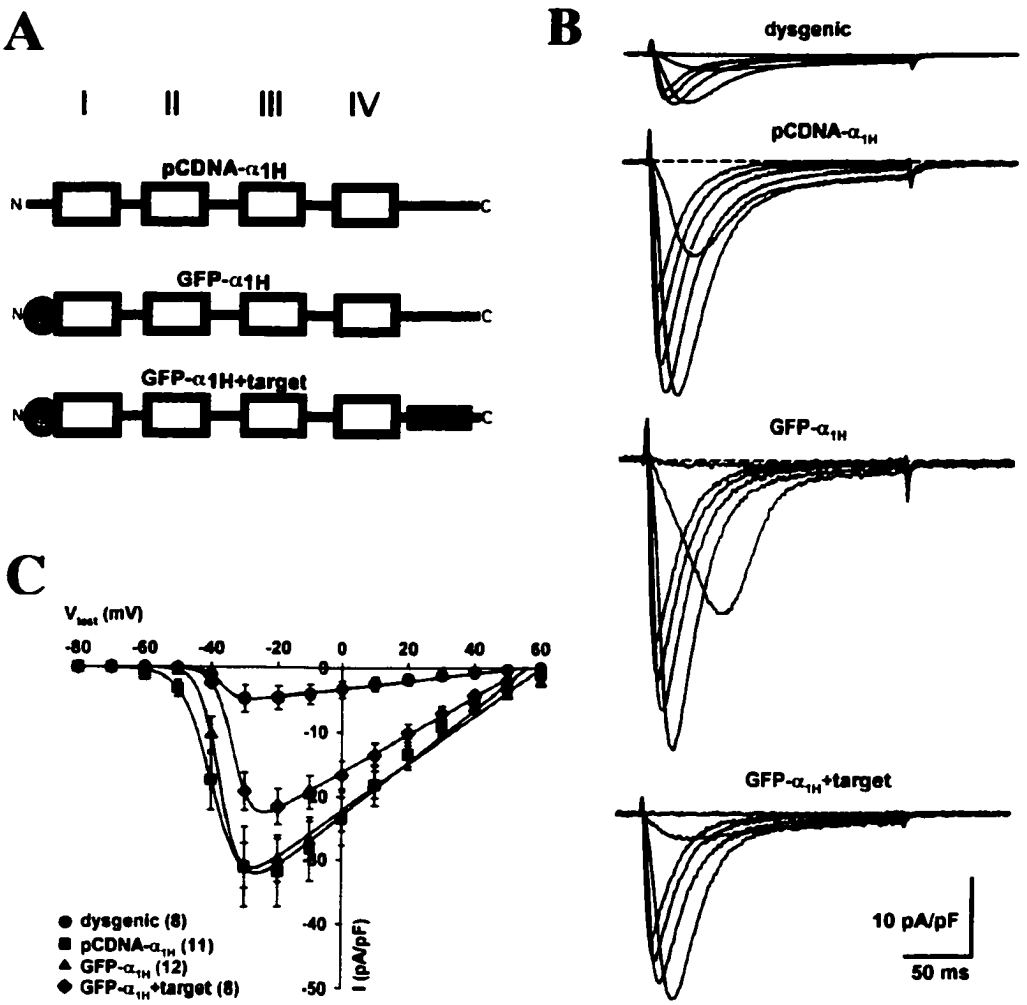

Figure 3.2. Cloned T-type channel constructs produce large Ca^{2+} currents in dysgenic myotubes. (A) Schematic representation of the α_{1H} channel constructs used in this study, where the open boxes represent homology repeats I-IV, circles indicate GFP coding sequence, and the solid box indicates the targeting sequence from α_{1S} ("target"; residues 1543-1662). (B) Representative whole-cell currents for native channels, or cloned constructs 24 hours after expression in dysgenic myotubes. Ca^{2+} currents elicited by 200 ms test depolarizations ranging from –50 mV to 0 mV were measured from a holding potential of –80 mV and superimposed to obtain a family of currents. (C) Average peak current-voltage relationships for native T-type channels (circles), or cloned channel constructs pCDNA-α_{1H} (squares), GFP-α_{1H} (triangles), and GFP-α_{1H}+target (diamonds) 24 hours after expression in dysgenic myotubes. The smooth lines represent fits of the average data to equation (1). Number of cells tested is given in parentheses.

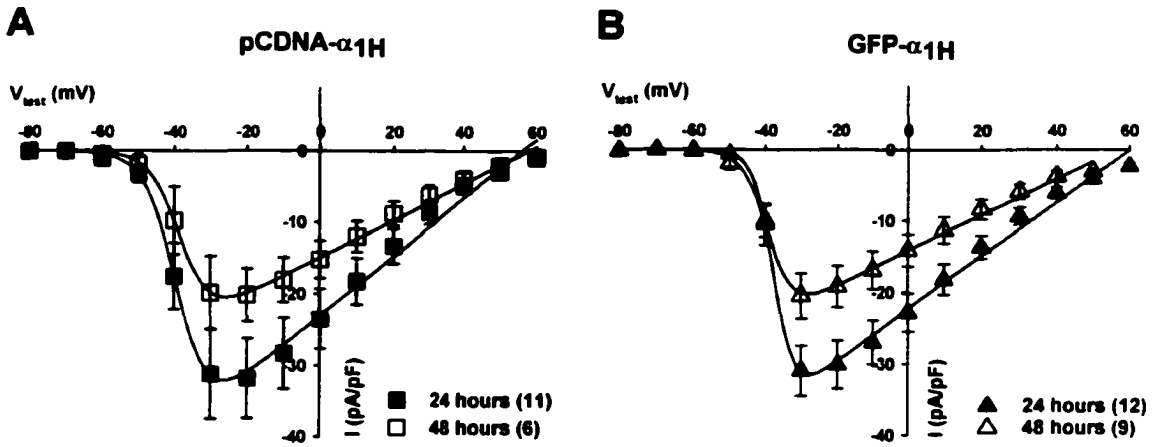

Figure 3.3. T-type Ca^{2+} current density follows a transient time course. Average peak current-voltage relationships for pCDNA-α_{1H} (A) or GFP-α_{1H} (B) 24 hours (filled symbols) and 48 hours (open symbols) after expression in dysgenic myotubes. The number of cells tested is given in parentheses. The smooth lines represent fits of the average data to equation (1). Number of cells tested is given in parentheses. For both constructs, Ca^{2+} current density peaked at 24 hours and declined by ~35% 48 hours after expression.

Ca^{2+} current density for α_{1H} constructs follows a transient time course

Because measurement of intramembrane charge movement for T-type Ca^{2+} channels is complicated by the presence of endogenous sodium and T-type Ca^{2+} channels in dysgenic myotubes, we measured whole-cell Ca^{2+} currents in order to examine expression levels of the T-type channel constructs. Figure 3.3 shows average peak current-voltage relationships for both "wild-type" constructs pCDNA-α_{1H} and GFP-α_{1H} 24 and 48 hours after expression in dysgenic myotubes. Ca^{2+} currents for both pCDNA-α_{1H} and GFP-α_{1H} followed a time course which peaked at about 32 pA/pF 24 hours after expression and declined by 35% to ~20 pA/pF after 48 hours (Fig. 3.3 A, B). This time course for current expression is also evident in the values of whole-cell conductance (G_{max}) calculated from peak currents (Table 3.1) for pCDNA-α_{1H} and GFP-α_{1H}. Since

TABLE 3.1

Activation parameters for native and cloned T-type Ca^{2+} channels in dysgenic myotubes

	dysgenic	pCDNA-α_{1H}		GFP-α_{1H}		GFP-α_{1H}+target	
	———	24 hr	48 hr	24 hr	48 hr	24 hr	48 hr
	(n=6-8)	(n=11)	(n=6)	(n=12)	(n=9)	(n=8)	(n=13)
G_{max} (nS/nF)	64 ± 23	437 ± 73	263 ± 43	403 ± 43	262 ± 37	294 ± 37	252 ± 29
V_R (mV)	49 ± 2	53 ± 2	57 ± 1	55 ± 2	53 ± 2	55 ± 1	54 ± 1
V_B (mV)	36 ± 1	36 ± 3	37 ± 3	37 ± 1	40 ± 2	34 ± 1	38 ± 1
k	3.1 ± 0.5	3.7 ± 0.6	3.3 ± 0.7	2.3 ± 0.3	2.5 ± 0.6	2.6 ± 0.5	2.1 ± 0.4

Average values for maximal conductance (G_{max}), reversal potential (V_R), half-maximal activation potential (V_B), and slope (k) were determined by fitting individual peak Ca^{2+} currents according to equation (1) and averaging over the number of cells tested. Measurements were taken approximately 24 or 48 hours after expression of cDNAs in dysgenic myotubes. Data are presented as mean ± SEM, with numbers in parentheses indicating the number of cells tested.

the GFP tag did not alter the time course or steady state activation parameters (Fig. 3.3, Table 3.1) of currents for pCDNA-α_{1H}, this provides additional evidence that the GFP fusion protein is not functionally different from the untagged wild-type construct.

Residues 1543-1662 of α_{1S} preserve expression of Ca^{2+} current density

Figure 3.4 illustrates average peak current-voltage relationships for GFP-α_{1H}+target 24 and 48 hours after expression in dysgenic myotubes. In contrast to both pCDNA-α_{1H} and GFP-α_{1H}, GFP-α_{1H}+target produced large Ca^{2+} currents which were maintained over a 48 hour period (I_{24}=21 pA/pF, I_{48}=20 pA/pF; n=8-12). Preservation of Ca^{2+} current density in the presence of "target" suggests that these residues may stabilize expression of the channel at the membrane.

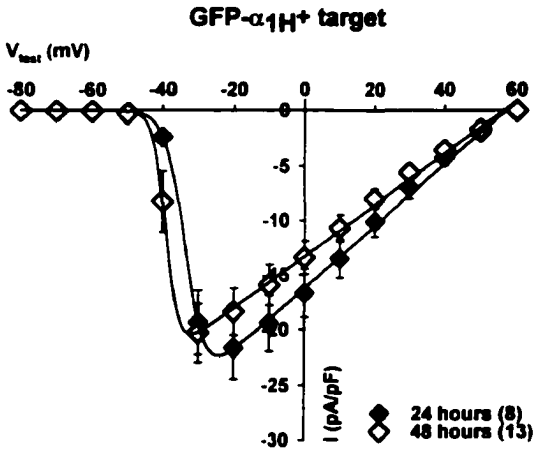

Figure 3.4. The presence of α_{1S} "target" at the C-terminus of α_{1H} stabilizes expression of Ca^{2+} current density. Average peak current-voltage relationships for GFP-α_{1H}+target 24 hours (filled diamonds) and 48 hours (open diamonds) after expression in dysgenic myotubes. The number of cells tested is given in parentheses. The smooth lines represent fits of the average data to equation (1). Number of cells tested is given in parentheses. Peak current densities at 24 and 48 hours are indistinguishable ($p > 0.1$).

Is GFP-α_{1H}+target able to target correctly to junctions?

If GFP-α_{1H}+target is able to reach junctions in dysgenic myotubes, this construct might restore some cardiac-type EC coupling (where Ca^{2+} influx through the α_{1C} activates the ryanodine receptor) in these cells. However, we found that neither pCDNA-α_{1H}, GFP-α_{1H}, nor GFP-α_{1H}+target were able to restore electrically evoked contractions in dysgenic myotubes (29-39 cells tested for each construct). Because the contribution of T-type Ca^{2+} current to the electrically evoked action potential may be too small to elicit Ca^{2+}-induced Ca^{2+} release, we also depolarized cells expressing GFP-α_{1H} or GFP-α_{1H}+target with square pulses at the peak of T-type Ca^{2+} current influx (-30 mV, 20-30 ms). However, both GFP-α_{1H} and GFP-α_{1H}+target produced slow, repeatable contractions in response to depolarizations (data not shown), suggesting that some channels are close enough to RyRs to evoke cardiac-type coupling, regardless of the presence of "target". Thus, we were unable to obtain a clear indication of whether or not GFP-α_{1H}+target is correctly targeted to junctions from these experiments.

As a final indication of targeting, we are currently attempting to produce a red fluorescent protein (dsRED) tagged α_{1S} subunit, which could then be colocalized with GFP-tagged channel constructs to determine whether two proteins exhibit similar subcellular distributions. We have successfully produced α_{1S} subunits with both C-terminal and N-terminal dsRED tags, and are now attempting to colocalize GFP-α_{1H}+target and dsRED-α_{1S}.

REFERENCES

Alberts, B., D. Bray, J. Lewis, M. Raff, K. Roberts, & J.D. Watson. (1994) Molecular Biology of the Cell; 3rd Edition. Garland Publishing, Inc.

Adams, B. A. & K. G. Beam. (1989) *J. Gen. Physiol.* 94: 429-444.

Adams, B. A., T. Tanabe, A. Mikami, S. Numa & K. G. Beam. (1990) *Nature* 346: 569-572.

Adams, B.A., Y. Mori, M.S. Kim, T. Tanabe, & K.G. Beam. (1994) *J. Gen. Physiol.* 104:985-96.

Bourinet, E., P. Charnet, W.J. Tomlinson, A. Stea, T.P. Snutch, & J. Nargeot. (1994) *EMBO (Eur. Mol. Biol. Organ.) J.* 13:5032-9.

Cachelin, A.B., J.E. de Peyer, S. Kokubun, & H. Reuter. (1983) *Nature (Lond.).* 304:462-4.

Casarotto, M. G., F. Gibson, S. M. Pace, S. M. Curtis, M. Mulcair & A. F. Dulhunty. (2000) *J. Biol. Chem.* 275: 11631-11637.

Cens, T., M.E. Mangoni, S. Richard, J. Nargeot, & P. Charnet. (1996) *Pflugers Arch. Eur. J. Physiol.* 431:771-4.

Cens, T., S. Restituito, A. Vallentin, & P. Charnet. (1998) *J. Biol. Chem.* 273:18308-15.

Costantin, J., F. Noceti, N. Qin, X. Wei, L. Birnbaumer, & E. Stefani. (1998) *J. Physiol.* 507:93-103.

Chaudhari, N. (1992) *J. Biol. Chem.* 267: 25636-25639.

Delcour, A.H., & R.W. Tsien. (1993) *Science.* 259:980-4.

DeMaria, C.D., T.W. Soong, B.A. Alseikhan, R.S. Alvania, & D.T. Yue. (2001) *Nature.* 411:484-489.

Dulhunty, A. F., D. R. Laver, E. M. Gallant, M. G. Casarotto, S. M. Pace & S. Curtis. (1999) *Biophys. J.* 77: 189-203.

El-Hayek, R., B. Antoniu , J. Wang, S. L. Hamilton, & N. Ikemoto. (1995) *J. Biol. Chem.* 270: 22116-22118.

El-Hayek, R. & N. Ikemoto. (1998) *Biochemistry* 37: 7015-7020.

Franzini-Armstrong, C. & F. Protasi. (1997) *Physiol. Rev.* 77: 699-729.

Flucher, B. E. & C. Franzini-Armstrong. (1996) *Proc. Natl. Acad. Sci. USA* 93: 8101-8106.

Flucher, B. E., N. Kasielke & M. Grabner. (2000) *J. Cell Biol.* 151: 467-477.

Flucher, B. E., S. B. Andrews & M. P. Daniels. (1994) *Mol. Biol. Cell.* 5: 1105-1118.

Gao, T., A. Yatani, M.L. Dell'Acqua, H. Sako, S.A. Green, N. Dascal, J.D. Scott, and M.M. Hosey. (1997) *Neuron.* 19:185-96.

Garcia, J. & K.G. Beam. (1994) *J. Gen. Physiol.* 103: 107-123.

Gee, S.H., R. Madhavan, S.R. Levinson, J.H. Caldwell, R. Sealock and S.C. Froehner. (1998) *J. Neurosci.* 18:128-37.

Giannini, G., A. Conti, S. Mammarella , M. Scrobogna & V. Sorrentino. (1995) *J. Cell Biol.* 128: 893-904.

Gollasch, M., J. Hescheler, J.M. Quayle, J.B. Patlak, & M.T. Nelson. (1992) *Am. J. Physiol.* 263:C948-52.

Grabner, M., A. Bachmann, F. Rosenthal, J. Striessnig, C. Schultz, D. Tautz & H. Glossmann. (1994) *FEBS Lett*, 339: 189-194.

Grabner, M., R. T. Dirksen & K. G. Beam. (1998) *Proc. Natl. Acad. Sci. USA* 95: 1903-1908.

Grabner, M., R. T. Dirksen, N. Suda, & K. G. Beam. (1999) *J. Biol. Chem.* 274: 21913-21919.

Grabner, M., Z. Wang, S. Hering, J. Striessnig, & H. Glossmann. (1996) *Neuron.* 16:207-18.

Hamill, O.P., A. Marty, E. Neher, B. Sakmann, & F.J. Sigworth. (1981) *Pflugers Arch. Eur. J. Physiol.* 391:85-100.

He, M., I. Bodi, G. Mikala, & A. Schwartz. (1997) *J. Biol. Chem.* 272:2629-33.

Hess, P., J.B. Lansman, & R.W. Tsien. (1984) *Nature (Lond.).* 311:538-44.

Hille, B. (1992) Ionic Channels of Excitable Membranes; 2nd Edition. Sinauer Associates Inc.

Hockerman, G.H., B.D. Johnson, M.R. Abbot, T. Scheuer, & W.A. Catterall. (1997) *J. Biol. Chem.* 272:18759-65.

Horton, R.M., H.D. Hunt, S.N. Ho, J.K. Pullen, & L.R. Pease. (1989) *Gene (Amst.).* 77:61-8.

Hoshi, T., & S.J. Smith. (1987) *J. Neurosci.* 7:571-80.

Ito, H., N. Klugbauer, & F. Hofmann. (1997) *Mol. Pharmacol.* 52:735-40.

Johnson, B.D., T. Scheuer, & W.A. Catterall. (1994) *Proc. Natl. Acad. Sci. USA.* 91:11492-6.

Kim, E., N. Martin, A. Rothschild, Y.N. Jan, and M. Sheng. (1995) *Nature* 378:85-88.

Kleppisch, T., K. Pedersen, C. Strubing, E. Bosse-Doenecke, V. Flockerzi, F. Hofmann, & J. Hescheler. (1994) *EMBO (Eur. Mol. Biol. Organ.) J.* 13:2502-7.

Knudson, C.M., N. Chaudhari, A.H. Sharp, J.A. Powell, K.G. Beam, & K.P. Campbell. (1989) *J. Biol. Chem.* 264:1345-8.

Kokubun, S., & H. Reuter. (1984) *Proc. Natl. Acad. Sci. USA.* 81:4824-7.

Lee, A., T. Scheuer, & W.A. Catterall. (2000) *J. Neurosci.* 20:6830-8.

Lew, W.Y., L.V. Hryshko, & D.M. Bers. (1991) *Circ. Res.* 69:1139-45.

Llinas, R.R., M. Sugimori, & B. Cherksey. (1989) *Ann. NY Acad. Sci.* 560:103-11.

Lu, X., L. Xu & G. Meissner. (1994) *J. Biol. Chem.* 269: 6511-6516.

Mikami, A., K. Imoto, T. Tanabe, T. Niidome, Y. Mori, H. Takeshima, S. Narumiya, & S. Numa. (1989) *Nature.* 340:230-3.

Mitterdorfer, J., Z. Wang, M.J. Sinnegger, S. Hering, J. Striessnig, M. Grabner, & H. Glossmann. (1996) *J. Biol. Chem.* 271:30330-5.

Mori, Y., T. Friedrich, M.S. Kim, A. Mikami, J. Nakai, P. Ruth, E. Bosse, F. Hofmann, V. Flockerzi, T. Furuichi, K. Mikoshiba, K. Imoto, T. Tanabe, & S. Numa. (1991) *Nature (Lond.).* 350:398-402.

Nakai, J., R. T. Dirksen, H. T. Nguyen, I. N. Pessah, K. G. Beam, & P. D. Allen. (1996) *Nature (London)* 380: 72-75.

Nakai, J., T. Tanabe, T. Konno, B. Adams & K. G. Beam. (1998) *J. Biol. Chem.* 273: 24983-24986.

Noceti, F., P. Baldelli, X. Wei, N. Qin, L. Toro, L. Birnbaumer, & E. Stefani. (1996) *J. Gen. Physiol.* 108:143-55.

Nowycky, M.C., A.P. Fox, & R.W. Tsien. (1985) *Proc. Natl. Acad. Sci. USA.* 82:2178-82.

Parri, H.R., & J.B. Lansman. (1996) *J. Neurosci.* 16:4890-902.

Pietrobon, D., & P. Hess. (1990) *Nature (Lond.).* 346:651-5.

Powell, J. A., L. Petherbridge & B. E. Flucher. (1996) *J. Cell Biol.* 134: 375-387.

Pragnell, M., M. De Waard, Y. Mori, T. Tanabe, T.P. Snutch, & K.P. Campbell. (1994) *Nature (Lond.).* 368:67-70.

Proenza, C., C. M. Wilkens & K. G. Beam. (2000) *J. Biol. Chem.* 275: 29935-29937.

Reuter, H. (1983) *Nature (Lond.).* 301:569-74.

Rios, E. & G. Brum. (1987) *Nature (London)* 325: 717-720.

Rittenhouse, A.R., & P. Hess. (1994) *J. Physiol.* 474:87-99.

Ruth, P., A. Rohrkasten, M. Biel, E. Bosse, S. Regulla, H.E. Meyer, V. Flockerzi, & F. Hofmann. (1989) *Science.* 245:1115-8.

Saiki,Y., R. El-Hayek & N. Ikemoto. (1999) *J. Biol. Chem.* 274: 7825-7832.

Sanguinetti, M.C., D.S. Krafte, & R.S. Kass. (1986) *J. Gen. Physiol.* 88:369-92.

Sather, W.A., T. Tanabe, J.F. Zhang, Y. Mori, M.E. Adams, & R.W. Tsien. (1993) *Neuron.* 11:291-303.

Schneider, M. F. & W. K. Chandler. (1973) *Nature (London)* 242: 244-246.

Sculptoreanu, A., A. Figourov, & W.C. De Groat. (1995) *Am. J. Physiol.* 269:C725-32.

Sculptoreanu, A., E. Rotman, M. Takahashi, T. Scheuer, & W.A. Catterall. (1993a) *Proc. Natl. Acad. Sci. USA.* 90:10135-9.

Sculptoreanu, A., T. Scheuer, & W.A. Catterall. (1993b) *Nature (Lond.).* 364:240-3.

Shieh, B.H. and M.Y. Zhu. (1996) *Neuron* 16:991-98.

Sinnegger, M.J., Z. Wang, M. Grabner, S. Hering, J. Striessnig, H. Glossmann, & J. Mitterdorfer. (1997) *J. Biol. Chem.* 272:27686-93.

Spaetgens, R.L., & G.W. Zamponi. (1999) *J. Biol. Chem.* 274:22428-36.

Takekura, H., M. Nishi, T. Noda, H. Takeshima and C. Franzini-Armstrong. (1995) *Proc. Natl. Acad. Sci. U.S.A.* 92:3381-85.

Takekura, H. and C. Franzini-Armstrong. (1999) *Dev. Dyn.* 214:372-80.

Tanabe, T., A. Mikami, T. Niidome, S. Numa, B.A. Adams, & K.G. Beam. (1993) *Ann. NY Acad. Sci.* 707:81-6.

Tanabe, T., B.A. Adams, S. Numa, and K.G. Beam. (1991) *Nature (Lond.).* 352:800-3.

Tanabe, T., H. Takeshima, A. Mikami, V. Flockerzi, H. Takahashi, K. Kangawa, M. Kojima, H. Matsuo, T. Hirose & S. Numa. (1987) *Nature (London)* 328: 313-318.

Tanabe, T., K. G. Beam, B. A. Adams, T. Niidome, & S. Numa. (1990) *Nature (London)* 346: 567-569.

Tanabe, T., K. G. Beam, J. A. Powell & S. Numa. (1988) *Nature (London)* 336: 134-139.

Tsien, R.W., D. Lipscombe, D.V. Madison, K.R. Bley, & A.P. Fox. (1988) *Trends Neurosci.* 11:431-8.

Wei, X., A. Neely, A.E. Lacerda, R. Olcese, E. Stefani, E. Perez-Reyes, & L. Birnbaumer. (1994) *J. Biol. Chem.* 269:1635-40.

Wilkens, C.M., M. Grabner and K.G. Beam. (2001a) *J. Gen. Physiol.* 118:495-507.

Wilkens, C.M., N. Kasielke, B.E. Flucher, K.G. Beam and M. Grabner. (2001b) *Proc. Natl. Acad. Sci. U.S.A.* 98:5892-7.

Zhang, J.F., A.D. Randall, P.T. Ellinor, W.A. Horne, W.A. Sather, T. Tanabe, T.L. Schwarz, & R.W. Tsien. (1993) *Neuropharmacology.* 32:1075-88.

Zhu, X., Gurrola, G., Jiang, M. T., Walker, J. W. & H. H. Valdivia. (1999) *FEBS Lett.* 450: 221-226.

Zühlke, R.D., G.S. Pitt, R.W. Tsien, & H. Reuter. (2000) *J. Biol. Chem.* 275:21121-9.